Hysteresis effects in magnetic nanoparticles: A simplified rate-equation approach

HYSTERESIS EFFECTS IN MAGNETIC NANOPARTICLES: A SIMPLIFIED RATE-EQUATION APPROACH

Paolo Allia [1,2], Gabriele Barrera [1], Paola Tiberto [1]

[1] *INRIM, Advanced Materials Metrology and Life Sciences, Strada delle Cacce 91, 10135 Torino (TO), Italy*

[2] *DISAT, Politecnico di Torino, Corso Duca degli Abruzzi 24, I-10129 Torino, Italy*

Abstract

Hysteretic properties of an assembly of uniaxial magnetic nanoparticles described as double well systems (DWS) with either collinear or randomly distributed easy axes are studied by means of a rate-equation approach. The resulting picture is sufficiently accurate to be exploited in high frequency applications of nanoparticles such as magnetic hyperthermia.

The rate equation scheme allows an exhaustive description of hysteretic effects to be achieved in a rather simple way, with remarkable advantages over treatments based on nonlinear equations of magnetization dynamics and models derived from the Stoner-Wohlfarth theory.

Rate equations for the magnetic DWS are then simplified and decoupled by making special assumptions on the escape frequency from the energy wells; it is shown that the simplified rate equation scheme can be applied in extended intervals of frequencies and temperatures, including the ones of interest for present-day practical applications of magnetic nanoparticles.

Analytical solutions of the simplified rate equations allow one to explain several hysteretic properties of the system when the magnetic field is applied either parallel or perpendicular to the nanoparticle easy axis. These solutions are suitable to be generalized to the case of an assembly of nanoparticles with randomly distributed easy axes.

Minor hysteresis loops of an assembly of DWS exhibit an anomalous behaviour: the magnetization driven by the periodic field initially follows a

spiral path in the (H, M) plane; closed, self-similar hysteresis loops corresponding to the system's steady state are achieved only after a sequence of iterations that depends on the loop's vertex field: the smaller the vertex field is, the longer the time needed to reach the steady state. Only major loops (i.e., ones where the magnetization goes from positive to negative saturation) are closed since the very beginning. The anomaly occurs at all angles between magnetic field and easy axis and at all explored frequencies. This effect should be taken in due account in magnetic hyperthermia experiments.

Keywords: Magnetic Nanoparticles, Two-Level Systems, Rate Equations, Hysteresis Loops

1. Introduction

Research on magnetic properties of ferro-/ferrimagnetic nanoparticles has anticipated the present-day, generalized interest towards nanophysics [1, 2]. The interest on quasi-static magnetic properties of ultrafine particles was first stimulated by the recognition of the peculiar magnetic effects originating from the reduction of size below a critical value [3] and was triggered by the need of understanding and optimizing the behavior of materials for magnetic recording [4].

More recently, the steadily increasing demand for new functional materials [5, 6, 7, 8, 9, 10, 11, 12, 13, 14, 15, 16, 17] has acted as a driving force for a great variety of experimental and theoretical studies on magnetic nanoparticles. The role of factors such as surface effects, particle size distribution, interparticle interaction, tendency to aggregation has been investigated and clarified in such a way that a commonly shared picture has gradually emerged [18, 19, 20, 21, 22, 23, 24]. On the other hand, dynamic magnetic properties of nanoparticles submitted to cyclic magnetization have become a hot topic in the last decade, in correspondence with the rise of interest towards biomedical applications such as magnetic hyperthermia [25, 26, 27, 28, 29, 30, 31, 32, 33].

However, a high applicative interest may hinder the progress of in-depth knowledge in favor of a simplified picture of the magnetic behavior of a nanoparticle assembly. The lack of an adequate theoretical description in the end may prevent the development of promising technical applications. This

work aims in particular to fill the gap of knowledge on magnetic hysteresis in uniaxial nanoparticles starting from the recognition that one's ability to explain the features of hysteresis loops is getting increasing importance in high frequency applications [33, 34, 35, 36, 37].

In a dilute assembly where interparticle interaction energy can be considered as a perturbation, the effect of thermal fluctuations on magnetic properties such as initial susceptibility, coercive force and magnetic remanence is generally understood in the context of the Néel model for thermally assisted (Arrhenius) magnetization reversal [38]. Uniaxial nanoparticles are described as classical double-well systems [39, 40] (DWS) where the particle's magnetic moment viewed as a macrospin [41, 42] switches between the energy minima.

Rate equations are a most natural way to picture the effects stemming from the redistribution of macrospins in the energy wells by effect of temperature and/or magnetic field. These equations can be rigorously derived [43] from the Fokker−Planck equation proposed by Brown [44, 45] for macrospin orientation under the condition that the DWS barrier be high enough at all temperatures of interest (anisotropy energy » thermal energy), as is often the case in real systems.

Rate equations have been exploited to reproduce the field-cooled (FC) and zero-field-cooled (ZFC) [41, 46] curves of initial susceptibility in monodisperse [47, 48, 49, 50] and polydisperse [39, 51] uniaxial nanoparticles. In DWS assemblies with randomly oriented easy axes, the difficulty of transforming rigorous results of numerical simulations in a simpler picture has been recently overcome by using a linearization that eases the description of FC/ZFC curves at low fields, allowing one to clarify the effects of cooling or heating rate, temperature, size distribution and magnetic field intensity on the behavior of FC/ZFC susceptibility [39].

A fortiori, rate equations are a most natural way to study magnetic hysteresis loops of a DWS assembly submitted to a time-dependent magnetic field. Actually, the canonical way to evaluate the dynamic evolution of magnetic structures at finite temperature implies solving the Landau-Lifshitz (LL) [52] or the Landau-Lifshitz-Gilbert (LLG) [53] equations. Brown′s equation itself can be derived from the stochastic LL/LLG equations[52]. How-

ever, analytical solutions of LL/LLG equations have been obtained in terms of continued fractions and not in closed form even in the case of uniaxial anisotropy [54], and numerical simulations [43, 55, 56] are so time-consuming that specific approximate approaches based, e.g., on Monte Carlo methods [53] must be developed.

Instead, a rate-equation approach to the dynamic behavior of a DWS assembly has the notable advantage of giving a sufficiently accurate picture of the system's evolution without requiring much computational power and time. Rate equations not only are an expedient analytical approximation of the more fundamental approach [45, 57, 58, 59], but also are suitable to be further simplified under specific conditions allowing one to get simple analytical laws for the behavior of physically significant hysteretic parameters such as coercive field and magnetic remanence. Their solutions are expected to hold over a rather extended interval of magnetizing frequencies and temperatures. For magnetic nanoparticles, rate equations were shown [44] to naturally emerge from the Fokker-Planck equation when the energy barrier of the DWS is significantly larger than thermal energy k_BT. In this paper, such a condition is fulfilled everywhere.

The effect of temperature on the coercive field of an assembly of DWS has been investigated in a number of papers based on a variety of approaches, including: i) the elementary Kneller's law [2, 60], ii) more advanced models involving suitable modifications of the Stoner-Wohlfarth (SW) theory, with the aim of either approximately accounting for the effect of thermal disorder[61, 62, 63] or simplifying the mathematical treatment [64], and iii) theories explicitly considering the dynamics of magnetic-moment redistribution between the two wells [52, 59]. Often, models are intended for collinear nanoparticles whose easy axis is parallel to the magnetic field; however, analytical [65] or numerical [52, 59, 61, 62, 63] expressions of the temperature-dependent coercive field for the case of a DWS assembly with randomly oriented easy axes do exist in the literature.

Typically, interaction among nanoparticles is neglected in the existing literature on hysteretic properties of magnetic nanomaterials [52, 59, 66]. Interparticle interaction influences the temperature dependence of the coercive field of SW nanoparticles in quasi-static conditions: in particular, it

has been shown that in a mean-field approach switching the interaction on causes the coercive field at a given temperature to increase with respect to the noninteracting case [67, 68]. However, the present knowledge on hysteretic magnetization in a nanoparticle assembly is so incomplete that the effect of interactions should be introduced only after the noninteracting case has been understood in all details.

In this paper, rate equations are used to study the hysteretic properties of a DWS assembly in quasi-static and high-frequency conditions over an extended temperature range (from above the blocking temperature to the $T \to 0$ limit) and under different vertex fields. Features, strong points and limiting factors of the method are discussed in some detail in Section 2.

Simplified rate equations are introduced and discussed in Section 3. Analytic solutions are derived for the special case of an assembly of DWS with collinear easy axes submitted to a field either parallel or perpendicular to the easy axis direction. In this case, the simpler symmetry of the problem allows one to get handy expressions of coercive field, magnetic energy, phase shift betheen magnetization and field waveforms and first magnetization curves. In this way, the underlying physics is easily understood. These analytical laws are shown to provide a more adequate representation of the system's properties with respect to the existing predictions based on simpler models.

The peculiar hysteresis effects emerging from the rate-equations framework are analyzed in Section 4. A specific anomaly is singled out and studied for an assembly of collinear DWS whose easy axis makes an arbitrary angle with the magnetic field direction, and shown to appear when magnetization follows a *minor* loop (i.e., one whose vertex field is not enough to bring the system to magnetic saturation). Initially, the trajectories of loops do not close on themselves and magnetization keeps spiralling in the (H, M) plane; in the end the steady state corresponding to closed magnetization loops is reached after a sequence of iterations that depends on the vertex field. The anomaly is not present in major loops (vertex field sufficient to reach magnetic saturation of the system). The effect is explained by analytical expressions obtained from the simplified rate equations.

Finally, the hysteretic properties of DWS assemblies with randomly directed easy axes are discussed in Section 5 for both quasi-static and high-

frequency major loops. Again, simplified rate equations are shown to play an important role in providing a simple expression of the coercive field as a function of temperature and frequency.

2. Cyclic Magnetization of double Well Systems: Definitions and Properties

2.1. Equations

Magnetic nanoparticles (NPs) with predominant uniaxial anisotropy are well described as double-well systems (DWS) [40]. In an assemby of noninteracting DWS the energy-well populations are determined by rate equations both at equilibrium and off-equilibrium [39, 51]. Features, advantages and limits of the classical DWS model applied to magnetic NPs were discussed elsewhere[39]. There, the study was limited to typical features of NPs submitted to a static magnetic field such as field cooled (FC) and zero field cooled (ZFC) susceptibilities. However, the model applies in non-static conditions as well and can therefore be exploited in order to study hysteresis loops displayed by blocked-particle systems submitted to cyclic magnetization. Here, the main aspects of the model are summarized and the main equations are expressed in dimensionless form.

Each magnetic nanoparticle is assumed to have size D and effective volume $V = (\pi/6)D^3$ and carries a magnetic moment $\mu = M_s V$ where M_s is the saturation magnetization of the material (macrospin approximation[41, 42]: atomic spins tightly coupled by exchange interaction and negligible surface effects); the magnetic moment is thought to be aligned by uniaxial anisotropy of amplitude K_{eff} to the easy axis. The easy directions of NPs are assumed to be evenly distributed in space; nevertheless, a simple planar representation is always able to fully describe the behavior of the magnetic moment[39]. In Figure 1a the plane containing the rotation of the μ vector is defined by the applied field H and the easy axis of a nanoparticle.

In real systems, magnetic nanoparticles are usually distributed in size according to a continuous law $p(D)$. The effects of a size distribution on the hysteretic properties of a DWS assembly will be discussed in Section 5.1.4; elsewhere monodisperse systems will be studied.

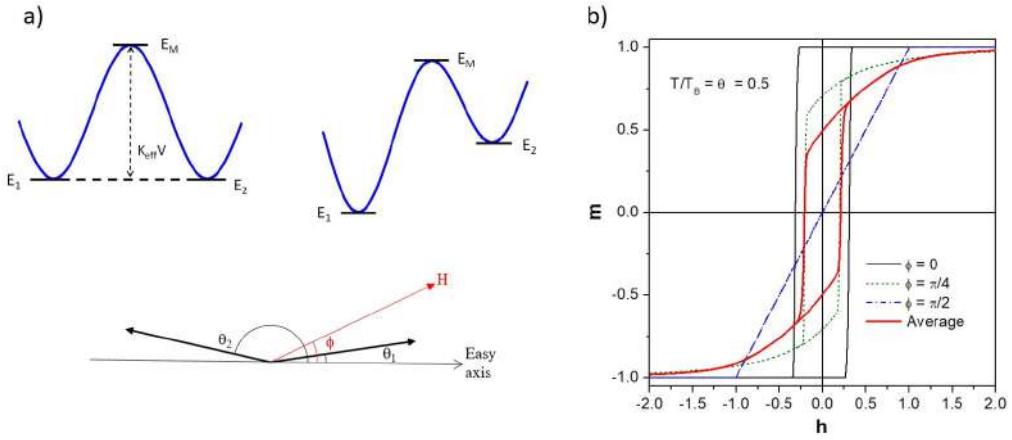

Figure 1: a) parameters of the rate-equation model for a DWS. Top sketch: DWS energy landscape without and with applied field; bottom image: reference system for the DWS (easy axis parallel to the x-axis); b) major hysteresis loops of blocked nanoparticles ($\Theta = 0.5$) obtained from rate equations for different values of angle ϕ and for an assembly of randomly oriented nanoparticles.

The blocking temperature T_B is defined as $K_{eff}V/ln(\tau_{meas}/\tau_0)k_B \approx$ $\approx K_{eff}V/25k_B$, where V is the NP volume, τ_{meas} is the typical measurement time (see Section 2.4 for details; in quasi-static conditions, $\tau_{meas} = 100$ s), $\tau_0 \approx 10^{-9}$ s is the reciprocal of the attempt frequency of a particle in an energy well [3]. In polydisperse systems, V must be substituted by the average NP volume $< V >$. In general, M_s and K_{eff} are functions of temperature; in this paper, both quantities are considered to be constant (the validity of such an assumption is discussed elsewhere [39]). Let N_ϕ be the number of particles of magnetic moment μ having an easy axis at an angle ϕ with respect to H; for symmetry reasons, only acute angles between H and the positive easy axis need to be considered (with reference to Fig 1a, $|\phi| \leq \pi/2$). For easy-axis directions evenly distributed in space $N_\phi = N/2\pi$, N being the total number of particles in the system. For each angle ϕ the occupancy numbers in the two wells are $N_{1\phi}$ and $N_{2\phi}$; here, the reduced quantities $n_{1\phi} = N_{1\phi}/N_\phi$ and $n_{2\phi} = N_{2\phi}/N_\phi$ will be used ($n_{1\phi} + n_{2\phi} = 1$). Moreover, the standard dimensionless magnetic quantities[3] will be introduced: $m(\phi) = M(\phi)/M_s =$

$M(\phi)/N_\phi\mu$, $h = HM_s/2K_{eff}$. We also define $\Theta = T/T_B$. The dimensionless energy of a single DWS, $\epsilon(\theta,\phi) = E(\theta,\phi)/K_{eff}V$ is given by:

$$\epsilon(\theta,\phi) = sin^2(\theta) - 2hcos(\theta-\phi)$$

where θ is the angle between the magnetic moment direction and the easy axis. The angles of minimum energy $\theta_1(\phi)$, $\theta_2(\phi)$ (see Figure 1a) are found by putting the derivative of $\epsilon(\theta,\phi)$ with respect to θ equal to zero; the magnetization along the field direction at the temperature Θ is therefore:

$$m(\Theta,\phi) = n_{1\phi}(\Theta)cos(\theta_1(\phi)-\phi) + n_{2\phi}(\Theta)cos(\theta_2(\phi)-\phi). \quad (1)$$

The redistribution of particles in the two wells of a DWS assembly is ruled by the rate equations[39]:

$$\begin{aligned}
\frac{dn_{1\phi}}{dt} &= -\frac{1}{\tau_1(t)}n_{1\phi} + \frac{1}{\tau_2(t)}n_{2\phi} = \frac{1}{\tau_2(t)} - \Big(\frac{1}{\tau_1(t)} + \frac{1}{\tau_2(t)}\Big)n_{1\phi} \\
\frac{dn_{2\phi}}{dt} &= \frac{1}{\tau_1(t)}n_{1\phi} - \frac{1}{\tau_2(t)}n_{2\phi} = \frac{1}{\tau_1(t)} - \Big(\frac{1}{\tau_1(t)} + \frac{1}{\tau_2(t)}\Big)n_{2\phi}.
\end{aligned} \quad (2)$$

In the standard Arrhenius picture the escape frequencies are $\tau_i^{-1} = \tau_0^{-1}exp\Big[-\frac{L}{\Theta}(\epsilon_M - \epsilon_i)\Big]$ $(i = 1,2)$ where $\epsilon_i(t)$ are the energies of the two energy minima, $\epsilon_M(t)$ is the energy at the top of the barrier(see Figure 1a), and $L = ln(\tau_0/\tau_{meas})$. The energies $\epsilon_{i,M}$ depend on time when $h = h(t)$. The problem's symmetry dictates the general relationship $\tau_1(-h) = \tau_2(h)$ that holds at all angles ϕ.

It should be explicitly noted that the double-well configuration depicted in Figure 1a is valid for $|h|$ values not larger than a maximum value $|h_{max}|$ that depends on angle ϕ (for $\phi = 0$ and $\phi = \pi/2$, $|h_{max}| = 1$). Actually, when $|h| > |h_{max}|$ the DWS collapses and only one energy well is left. For a generic angle ϕ the rate equations must be numerically solved (details of the forward Euler method are given elsewhere [39]); a first example of the features of the DWS model applied to a cyclic magnetization process is given in Figure 1b, where

three major hysteresis loops are plotted for an assembly of monodisperse nanoparticles submitted to a magnetic field linearly decreasing/increasing in time well below blocking temperature. Further considerations about role and representation of the rate of change of $h(t)$ in cyclic conditions are reported in Section 2.2

The curves of Fig. 1b are similar to but not coincident with the ones obtained from the standard Stoner-Wohlfarth (SW) model [1] where the changes between $n_{1\phi}$ and $n_{2\phi}$ are not considered as produced by a thermally activated process: they are assumed to occur when the absolute value of the applied field reaches $|h_{max}|$ and only one energy minimum remains.

The rate equations are considerably simplified when $\phi = 0$, so that it becomes possible to solve them and to derive analytic expressions which help understanding the underlying physics (see Sections 2.3 and 3). Finally, when $\phi = \pi/2$ the occupancy numbers $n_{1\,\pi/2}$ and $n_{2\,\pi/2}$ never change, so that the rate equations reduce to $dn_{1\,\pi/2}/dt = dn_{2\,\pi/2}/dt = 0$.

2.2. Measurement Time and Sweep Rate in Cyclic Measurements

Measurement time plays a central role in NP magnetism. In static conditions, τ_{meas} determines the magnetic regime (whether blocked or superparamagnetic) of the system at a given temperature [69]. Measurement time also has effect on the time evolution of a DWS assembly during the cyclic magnetization process. In this case however, a further parameter is to be considered, i.e., the rate of change of the magnetizing field $h(t)$ (sweep rate). In the recent literature on high-frequency effects, the sweep rate is sometimes assumed to be proportional to τ_{meas}^{-1} [66, 70]. However, such an identification is far from being general if one makes reference to the experimental practice.

Hysteresis loops on NP systems are usually measured in two distinctly different experimental conditions: a) quasi-static measurements are done using e.g. a Vibrating-Sample Magnetometer or a SQUID Magnetometer; b) frequency measurements are done using e.g. a BH Tracer based on the induction principle:

a) in the quasi-static case the sweep rate of h is largely independent of τ_{meas}. The magnetic field is automatically modified by the instrument at a nominal, built-in rate; after reaching each target value the field is kept constant

for a fixed time ($= \tau_{meas}$) in order to measure the magnetization of sample with due accuracy; then the field is changed again. The whole procedure is therefore composed of a sequence of measurements at fixed field separated by fast changes of h at the nominal sweep rate of the instrument. As a first approximation, the field can be assumed to change from an upper vertex (h_v) to a lower vertex ($-h_v$) and viceversa according to the linear law $h(t) = h(0) \pm rt$, where $h(0)$ is the initial value of the dimensionless field, r is the average sweep rate in quasi-static measurements, defined as $2h_v/\Delta t$ (Δt being the total time taken by the instrument to do all measurements from the upper to the lower vertex) and is considered constant over the whole interval. This rate is a positive quantity, and the $\pm$ sign refer to the lower/upper branch of the hysteresis loop. Therefore, in magnetometric measurements there is basically no strict relation between sweep rate and measurement time: the two parameters must be kept distinct.

b) in high frequency measurements τ_{meas} is conventionally taken as the reciprocal of measurement frequency f [66, 71]. In this case the sweep rate is no longer a constant; nevertheless, it is still possible to introduce a r.m.s sweep rate r_{RMS} defined as $r_{RMS} = (\pi/\sqrt{2})h_v f$ where h_v is the dimensionless vertex field. In the literature, slightly different expressions for the r.m.s. rate have been proposed f [66, 72]; however the above expression is more adequate to treat the case of a sinusoidal $h(t)$ waveform. The dimensionless rate equations (2) can be easily rewritten in terms of the dimensionless field h:

$$\begin{aligned} \frac{dn_{1,\phi}}{dh} &= \mp\frac{1}{r}\Big[\frac{1}{\tau_2(h)} - \Big(\frac{1}{\tau_1(h)} + \frac{1}{\tau_2(h)}\Big)n_{1,\phi}\Big] \\ \frac{dn_{2,\phi}}{dh} &= \mp\frac{1}{r}\Big[\frac{1}{\tau_1(h)} - \Big(\frac{1}{\tau_1(h)} + \frac{1}{\tau_2(h)}\Big)n_{2,\phi}\Big]. \end{aligned} \tag{3}$$

where $r \to r_{RMS}$ in frequency measurements and the $\mp$ sign refers to the upper/lower loop branch.

2.3. Simplified Rate Equations

An analytically manageable form of the full rate equations is obtained by neglecting $1/\tau_1$ for $h > 0$ and $1/\tau_2$ for $h < 0$ in Eq. 3; in this way, two independent equations are obtained for positive and negative values of h:

$$\begin{aligned} \frac{dn_{1,\phi}}{dh} &= \pm\frac{1}{r\tau_1(h)}n_{1,\phi} \qquad h < 0 \\ \frac{dn_{2,\phi}}{dh} &= \pm\frac{1}{r\tau_2(h)}n_{2,\phi} \qquad h > 0 \end{aligned} \tag{4}$$

where the $\pm$ sign refers to the upper/lower loop branch. In both regions of h the evolution of the complementary occupancy number is determined by the relation $dn_{2\phi}/dh = -dn_{1\phi}/dh$.

The approximation amounts to assume that particles in energy minimum 1(2) of the double well do not leave the minimum when $h > 0$ (< 0), and holds when both wells are sufficiently deep at $h = 0$, i.e., when $r\tau_1(0) = r\tau_2(0) = r\tau_0 exp(L/\Theta) \gg 1$. In high frequency measurements, L changes to $L_f = ln(1/(f\tau_0))$ and the blocking temperature T_{Bf} increases with respect to the one resulting from quasi-static measurements (see Supplementary Material [73], Section 1); however, the ratio $L_f/(T/T_{Bf}) \equiv L_f/\Theta_f$ is independent of f and is always equal to the ratio L/Θ, as shown in the Supplementary Material. The above condition leads to the following inequality for the temperature Θ in order to make use of the simplified equations:

$$\Theta < \frac{L}{ln\left(\frac{1}{r\tau_0}\right)} = \frac{L}{ln\left(\frac{\sqrt{2}}{\pi f\tau_0}\right)} \tag{5}$$

The right-side quantity takes values ranging from 1.27 for $f = 1$ Hz to 6.65 for $f = 10$ MHz; therefore, simplified rate equations can be exploited below the static blocking temperature and can be used even well above, depending on frequency. Applications of the simplified rate equations will be discussed in the following Sections.

2.4. Limiting Factors in the Treatment of Magnetic Hysteresis by the DWS Model

The area of a magnetization loop $m(h)$ (such as the ones shown in Figure 1b) is equal to the dimensionless energy ϵ released by the DWS assembly towards the surrounding environment. At a finite temperature the energy is released by the combined effect of thermal activation and magnetic field, which causes an imbalance between $1 \rightarrow 2$ and $2 \rightarrow 1$ transition probabilities; specifically, transitions from the energy minimum higher in energy towards the one lower in energy prevail and the associated net energy flux equals the energy lost to the environment. However, the hysteresis loss predicted by the DWS model (as well as by the SW model) does not account for *all* microscopic mechanisms of energy loss (as, e.g., dissipation of eddy currents generated within each nanoparticle). Moreover, the model does not enter the details of the actual dynamics of the reversing macrospin during the transition from one double-well minimum to the other; in fact, macrospin reversal is considered to instantaneously take place once it is initiated by activation. This is of course an oversimplification because the actual magnetic-moment reversal should follow a magnetization-dynamics equation such as the Landau-Lifshitz-Gilbert equation [69].

An operational limit of the rate equation model applied to a DWS assembly, partially related to the previous considerations, appears when high-frequency measurements are considered. By definition the highest escape frequency in the Arrhenius formalism is $\tau_0^{-1} \approx 1 \times 10^9$ Hz. As a consequence, the DWS assembly becomes increasingly non-responding as f approaches such a limit; the highest frequency studied in this work is therefore $f = 1 \times 10^7$ Hz (for minor loops). This limit of the rate equation model was already acknowledged [72]. At higher frequencies, the model is no longer adequate and should be substituted by other approaches able to account for faster changes of magnetization.

Despite these limits and criticalities, the rate equation model permits notable advances in knowledge and application of magnetic nanoparticles in dynamical conditions and has many advantages with respect to more simplified treatments of cyclic magnetization processes, as shown in the next Sections.

3. Analytic Expressions for $\phi = 0$ and $\phi = \pi/2$

Although the NP easy axes in a real system usually point at random along all directions in space, the response of a DWS assembly with aligned easy axes is a most interesting study case, because it allows one to derive approximate rate equations and to find analytical solutions when the magnetic field is applied either parallel ($\phi = 0$) or perpendicular ($\phi = \pi/2$) to the common easy axis of nanoparticles.

3.1. Energies and Time Constants

When $\phi = 0$, the energies ϵ_i, ϵ_M are:

$$\epsilon_1 = -2h, \quad \epsilon_M = 1 + h^2, \quad \epsilon_2 = 2h \tag{6}$$

so that the time constants τ_i become:

$$\tau_1 = \tau_0 e^{\frac{L}{\Theta}(1+h)^2}, \quad \tau_2 = \tau_0 e^{\frac{L}{\Theta}(1-h)^2}$$

When $\phi = \pi/2$ the energies are:

$$\epsilon_1 = \epsilon_2 = -h^2, \quad \epsilon_M = 1 - 2h \tag{7}$$

resulting in identical time constants:

$$\tau_1 = \tau_2 = \tau_0 e^{\frac{L}{\Theta}(1-h)^2}$$

3.2. Solutions of the Simplified Rate Equations for $\phi = 0$

When $\phi = 0$ the simplified rate equations (4) admit the solutions:

$$
\begin{aligned}
n_{10}(h) &= n_{10}(h_i)exp\Big(\pm \frac{1}{r}\int_{h_i}^{h} \frac{1}{\tau_1}dh\Big) \\
&= n_{10}(h_i)exp\Big(\pm \frac{1}{r\tau_0}\int_{h_i}^{h} e^{-\frac{L}{\Theta}(1+h)^2}dh\Big) \qquad h<0 \\
n_{20}(h) &= n_{20}(h_i)exp\Big(\pm \frac{1}{r}\int_{h_i}^{h} \frac{1}{\tau_2}dh\Big) \\
&= n_{20}(h_i)exp\Big(\pm \frac{1}{r\tau_0}\int_{h_i}^{h} e^{-\frac{L}{\Theta}(1-h)^2}dh\Big) \qquad h>0
\end{aligned}
\tag{8}
$$

where h_i is the initial value of h and again the $\pm$ sign refers to the upper/lower loop branch. These solutions will be exploited in the following Sections.

When $\phi = \pi/2$ the populations in the two wells are equal and constant, both below and above $\Theta = 1$.

3.3. Coercive Field

Let us refer to the upper half of a major loop, with h taking values from the positive vertex field $h_v = 1$ to $h_v = -1$. From the approximate rate equations, it is possible to obtain an analytic expression of the coercive field. The coercive field h_c is a negative quantity in this case, so that the first of the Equations (8) must be used. The resulting expression for h_c is (see Supplementary Material [73], Section 2, for details):

$$
h_c = -1 + \Big(\frac{\Theta}{L}\Big)^{1/2} erf^{-1}\Big(1 - \frac{2}{\sqrt{\pi}}\Big(\frac{L}{\Theta}\Big)^{1/2}\tau_0 r ln2\Big)
$$

where $erf^{-1}(y)$ is the inverse error function of argument $y = 1 - x = 1 - \Big[\frac{2}{\sqrt{\pi}}\Big(\frac{L}{\Theta}\Big)^{1/2}\tau_0 r ln2\Big]$. The quantity x is always very small, so that an

approximate expression of the erf^{-1} function [74] can be used, resulting in the following analytically manageable expression for $|h_c|$:

$$|h_c| = 1 - \left(\frac{\Theta}{L}\right)^{1/2} \left[-\frac{2}{\pi a} - \frac{ln(2x)}{2} + \sqrt{\left(\frac{2}{\pi a} + \frac{ln(2x)}{2}\right)^2 - \frac{ln(2x)}{a}} \right]^{1/2} \quad (9)$$

where $a \approx 0.14$ [74]. It should be noted that this expression is valid not only in quasi-static measurements but also at high magnetizing frequency (with the only proviso that the r.m.s. rate r_{RMS} substitute the static rate r). The behavior of $h_c(\Theta)$ is shown in Figure 2 for various values of frequency, including quasi-static measurements. For each frequency, the lines correspond to the approximate expression (9) and the symbols to the value of h_c obtained by numerically integrating the full rate equations (3). As expected, the agreement between the two sets of data is always excellent for all values of Θ compatible with condition (5).

According to Equation (9), h_c is not zero at $\Theta = 1$ (i.e., at the blocking temperature) even in quasi-static measurements (full symbols in Figure 3). As a matter of fact, h_c only disappears at temperatures where thermal equilibrium is reached by the system, as clearly shown in Figure 3. There, the behavior of the coercive field of a quasi-static loop is plotted together with the ZFC susceptibility curve and the corresponding equilibrium susceptibility[39] in the region around $\Theta = 1$. As known, the distance of the ZFC susceptibility from the equilibrium value measures how far the nanoparticle system is from thermal equilibrium. Indeed, h_c disappears exactly when the ZFC curve (full line) merges with the equilibrium curve (dashed line).

The present analytic expression for h_c has the same structure as the formula obtained in the simplest approach to coercive field of collinear NPs with $\phi = 0$ [60], i.e., $h_c = 1 - \Theta^{1/2} = 1 - (T/T_B)^{1/2}$ (Kneller's law), which however fails to account for the actual behavior of h_c near to blocking temperature. As a matter of fact, any expression not containing the magnetizing frequency or the field sweep rate cannot fit the behavior of $h_c(\Theta)$ predicted by the rate equation model. Furthermore, Equation (9) is more accurate (particularly at high frequencies) than the corresponding expression proposed by Usov [59].

As clearly shown in Figure 2, the analytic expression for h_c provides a

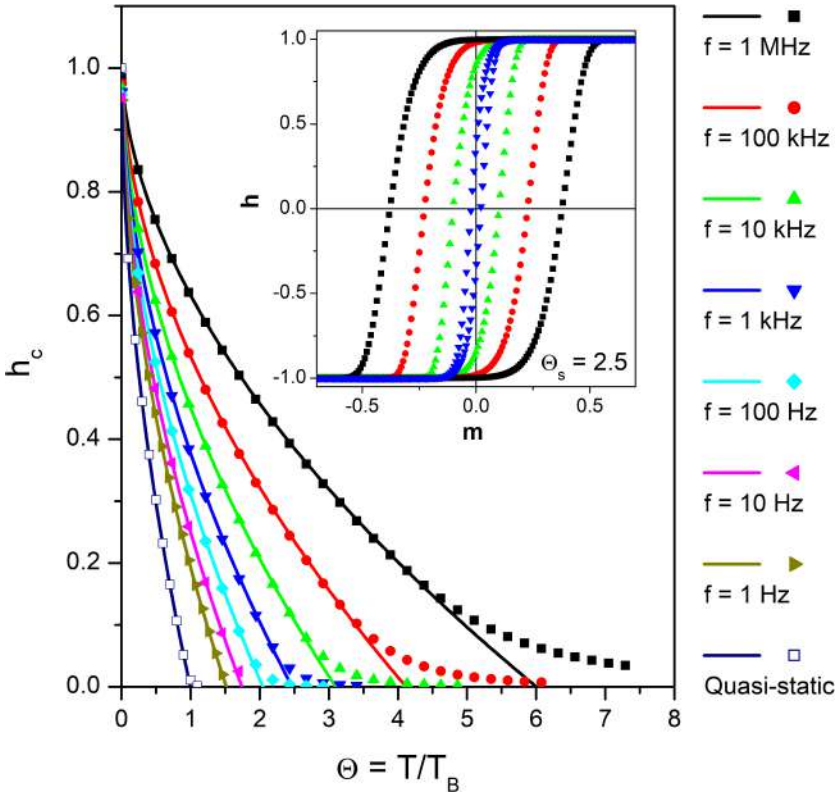

Figure 2: Symbols: temperature behavior of the coercive field of collinear monodisperse nanoparticles ($\phi = 0$) at different magnetizing frequencies, resulting from the full rate equations; full lines: approximate analytical law (Equation (9). Inset: hysteresis loops appearing at high frequencies well above the static blocking temperature.

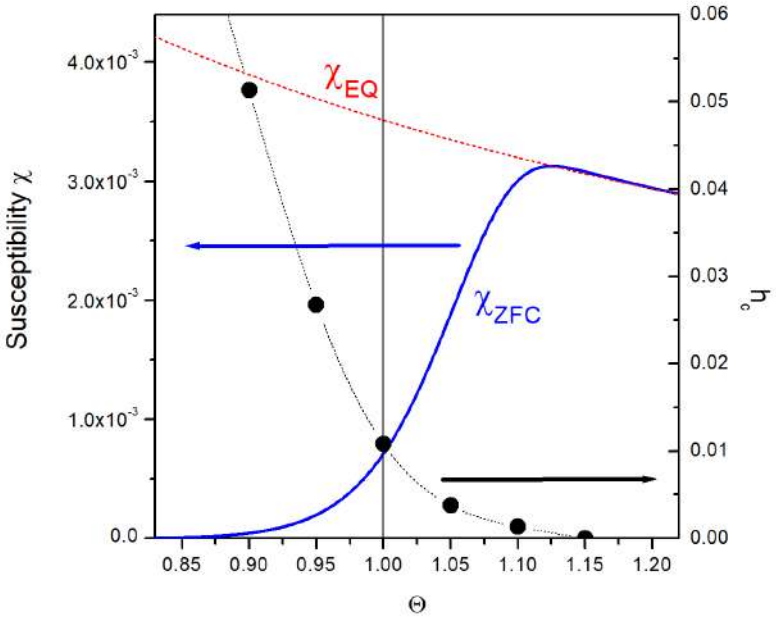

Figure 3: Coercive field h_c (symbols), ZFC susceptibility χ_{ZFC} (blue full line) and equilibrium susceptibility χ_{EQ} (red dotted line) around blocking temperature for collinear monodisperse nanoparticles ($\phi = 0$).

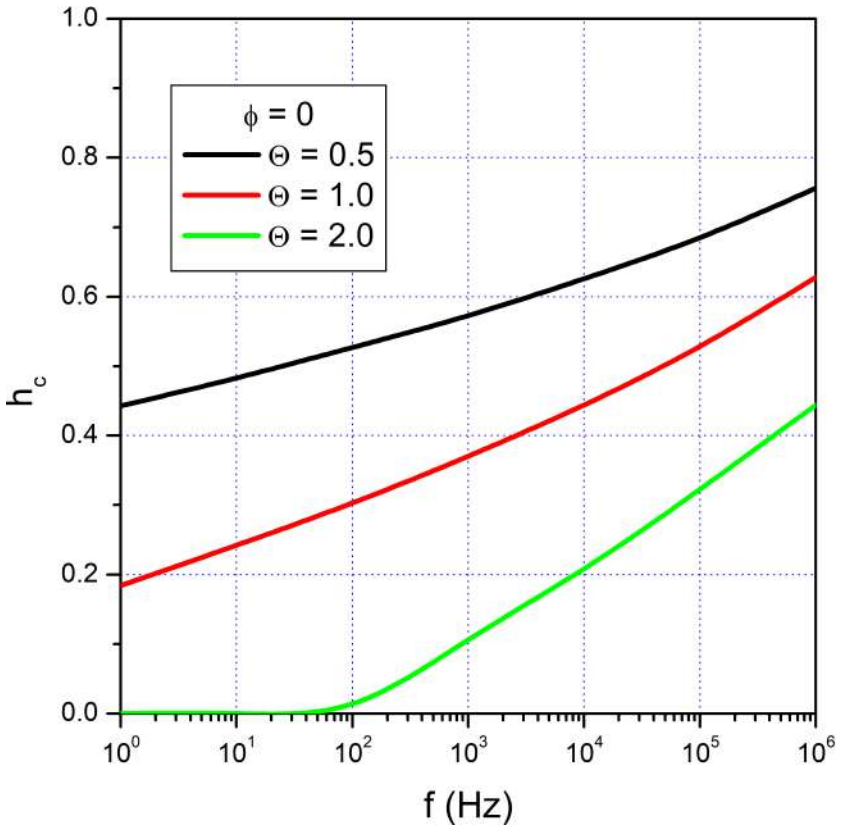

Figure 4: Coercive field as a function of magnetizing frequency for collinear monodisperse nanoparticles ($\phi = 0$) at three temperatures.

good approximation of the exact value at almost all temperatures Θ and at all investigated frequencies, and can be exploited to evaluate how much does h_c increase with increasing f, as shown in Figure 4 for three values of Θ. In particular, when $\Theta \gg 1$ quasi-static and low-frequency curves become fully reversible ($h_c = 0$), as expected; however, a hysteresis loop opens at higher frequencies. An example is reported in the inset of Figure 2 where the hysteresis loops for $f \geq 10^3$ Hz are shown at $\Theta = 2.5$; magnetization curves taken at lower frequencies are reversible.

When $\phi = \pi/2$ the $m(h)$ curve displays no hysteresis.

3.4. Energy Stored in the DWS assembly

The general expression of the total energy of a DWS assembly is:

$$\epsilon = n_{1\phi}\epsilon_1 + n_{2\phi}\epsilon_2$$

When $\phi = 0$ the magnetization (Equation(1)) becomes:

$$m = 2n_{10} - 1 = 1 - 2n_{20} \tag{10}$$

and the total energy can be written:

$$\epsilon = -2h(n_{10} - n_{20}) = -2hm$$

where use has been made of Equations (6) and (10). Temperatures below and above $\Theta = 1$ are separately considered:

a) below Blocking Temperature

When $\Theta < 1$ the values of n_{10} and n_{20} can be obtained from the simplified rate equations (4). The left-side panels of Figure 5 show energy and magnetization for $\phi = 0$, $\Theta = 0.5$ for the upper branch of a major hysteresis loop (full black lines; for clarity's sake the lower branch of both $m(h)$ and $\epsilon(h)$ are also shown as dotted lines). In this case, the magnetic field decreases from $h_v = +1$ to $-h_v = -1$. When $h = +1$, only one energy minimum (1) exists and the system's Zeeman energy is minimized. When h is reduced the second energy minimum (2) appears, but is initially empty because the quantity $r\tau_1$ is so large that $dn_{10}/dt \simeq 0$. When the field becomes negative, the energy is no longer minimized; however, initially $r\tau_1$ is still so large that the $1 \rightarrow 2$ transitions are inhibited. A positive magnetic energy equal to $2n_{10}h$ (in standard units, $N_{10}\mu H$ erg/cm^3) is stored in the system. Around $-|h_c|$ the quantity $r\tau_1$ suddenly drops (and simultaneously $r\tau_2$ strongly increases) so that the $1 \rightarrow 2$ transition processes become dominant, until the energy well (1) is completely emptied. The stored magnetic energy is quickly released by the ensemble to the environment as heat and the energy of the DWS assembly is again minimized.

b) above Blocking Temperature

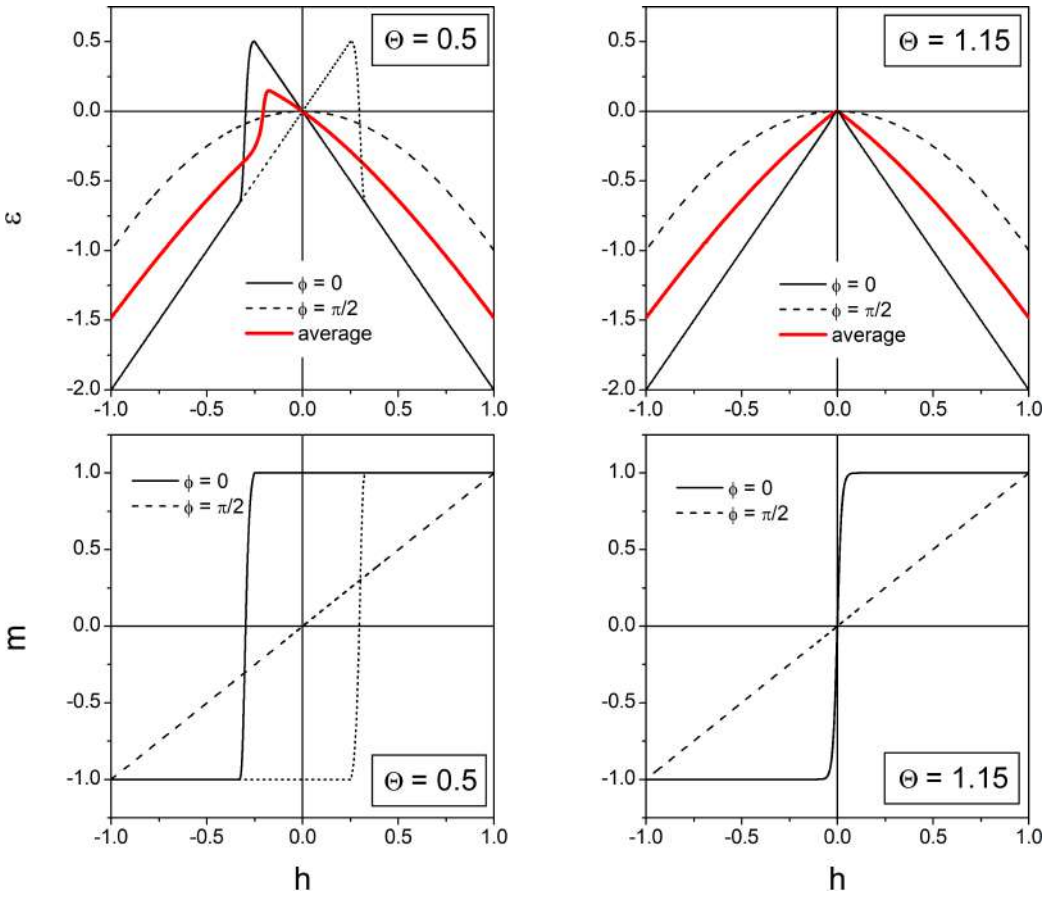

Figure 5: Left panels: behavior of energy ϵ and magnetization m on the upper branch of a major loop well below blocking temperature for collinear monodisperse nanoparticles (black full lines: $\phi = 0$, black dashed lines: $\phi = \pi/2$); behavior of ϵ for an assembly of monodisperse nanoparticles with random easy axes (red line). Right panels: the same quantities above blocking temperature.

In this case, the full rate equations must be used because condition (5) is no longer fulfilled. The full lines in the right-side panels of Fig. 5 show energy and magnetization above blocking temperature ($\Theta = 1.15$). As expected, the hysteresis loop disappears, and no magnetic energy accumulation is observed. Here $n_{10} = \frac{1}{1+e^{-\alpha}}$ and $n_{20} = \frac{e^{-\alpha}}{1+e^{-\alpha}}$ are the equilibrium occupancy values [39], and $\alpha = (L/\Theta)(\epsilon_2 - \epsilon_1) = 4(L/\Theta)h \approx 100h$; therefore the energy becomes:

$$\epsilon = -2h\frac{1 - e^{-\alpha}}{1 + e^{-\alpha}} \approx -2h$$

the latter approximate equality being valid almost everywhere on the h axis because $\alpha \gg 1$ with the exception of a narrow region around $h = 0$ where the $\epsilon(h)$ curve continuously changes its slope without exhibiting a cusp. When $\phi = \pi/2$ the magnetization (Equation (1)) becomes:

$$\begin{aligned} m &= -1 \qquad h < -1 \\ m &= h \qquad -1 \leq h \leq 1 \\ m &= +1 \qquad h > 1 \end{aligned}$$

and the total energy is written, using Equation (7) :

$$\epsilon = (n_{1\pi/2} + n_{2\pi/2})\epsilon_1 = \epsilon_1 = -h^2$$

In this case, there is no difference between the curves taken above and below blocking temperature, as shown in Fig. 5 (dashed black lines in the upper panels).
A discussion about the phase shift occurring between driving field and magnetization in high-frequency measurements is given in the Supplementary Material [73], Section 3.

3.5. Curves of First Magnetization at Different Temperatures and Frequencies

The DWS assembly is now considered to be initially in the demagnetized state ($h = 0$, $m = 0$, $n_{10} = n_{20} = 1/2$). The field is increased from $h = 0$ to $h = 1$. The second simplified rate equation (4) applies; the solution with the

minus sign in the argument of the exponential must be used in the present case:

$$n_{20}(h) = \frac{1}{2} exp\Big(- \frac{1}{r_{RMS}} \int_0^h \frac{1}{\tau_2} dh \Big)$$

so that by Equation (10)

$$m(h) = 1 - e^{-\frac{1}{r_{RMS}} \int_0^h \frac{1}{\tau_2} dh}. \tag{11}$$

As shown in the Supplementary Material [73], Section 4 , Equation (11) can be transformed into:

$$m(h) = 1 - e^{-\beta(h)}$$

$$\beta(h) = \frac{\sqrt{\pi}}{2} \frac{1}{\tau_0 r_{RMS}} \Big(\frac{\Theta}{L}\Big)^{1/2} \Big\{ erf\Big[\Big(\frac{L}{\Theta}\Big)^{1/2}\Big] - erf\Big[\Big(\frac{L}{\Theta}\Big)^{1/2}(1-h)\Big]\Big\} \tag{12}$$

$$\simeq \frac{\sqrt{\pi}}{2} \frac{1}{\tau_0 r_{RMS}} \Big(\frac{\Theta}{L}\Big)^{1/2} \Big\{ 1 - erf\Big[\Big(\frac{L}{\Theta}\Big)^{1/2}(1-h)\Big]\Big\}$$

where erf is the error function and $0 \leq h \leq 1$. The assumption $erf\Big[\Big(\frac{L}{\Theta}\Big)^{1/2}\Big] \simeq 1$ is allowed because the argument is considerably larger than unity for all Θ values of interest. Note that the first magnetization curve depends on frequency only through the rate r_{RMS}. A set of curves at two fixed temperatures and at different frequencies have been obtained using the approximation of the erf function[75, 76] given in the Supplementary Material [73], Section 5, and are shown in Figure 6 (full lines for $\Theta = 0.5$, dashed lines for $\Theta = 2$). The validity of the simplified rate-equation approach has been verified by comparing the curves for $f = 100$ kHz with the results obtained by solving the full rate equations (Equation (3)) at both temperatures (circles in Figure 6): the agreement is excellent. At $\Theta = 2$, however, the simplified rate equations and Equation (12) can be used only above 100 Hz, as required by Equation (5).

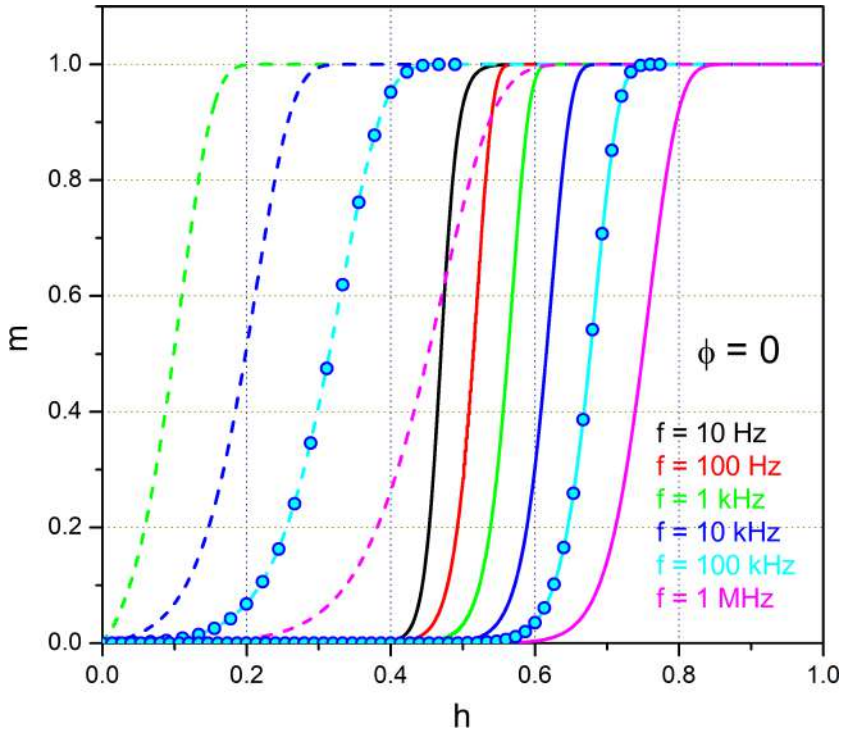

Figure 6: Curves of first magnetization for collinear monodisperse nanoparticles ($\phi = 0$) at two temperatures (full lines: $\Theta = 0.5$, dashed lines: $\Theta = 2$) obtained from Equation (12) for different magnetizing frequencies. Symbols: first magnetization curves resulting from integration of the full rate equations.

4. Minor Loops and Initial Loop Anomaly for an Arbitrary Angle ϕ

When the vertex field h_v is less than unity in absolute value, the magnetization of a DWS assembly follows a symmetric *minor* loop [70]. In principle, $|h_v|$ can take any value between 0 and 1 for any angle ϕ between the easy axis and the magnetic field; the latter is oscillating between h_v and $-h_v$ at a fixed frequency f. The study of minor loops is not only interesting *per se* (in high-frequency measurements one usually deals with minor loops [70, 77]), but also because of a remarkable effect appearing in a DWS assembly submitted to cyclic magnetization. As a matter of fact, when the magnetization begins to follow a minor loop at a given frequency f starting from the demagnetized state ($m = 0$), the steady state characterized by stable, self-similar closed loops is reached only after a sequence of iterations that depends on the value of vertex magnetization $m_v = m(h_v)$.

A typical example of such an anomaly is shown in the top panels of Figure 7. The top left panel shows minor hysteresis loops of collinear nanoparticles obtained by solving the full rate equations for $\phi = 0$ starting from the demagnetized state. The first magnetization curve up to h_v (indicated by label 0) is followed by a sequence of loops (numbered by $1, 2, 3, ..$) whose trajectories do not to close on themselves and keep spiralling in the (h, m) plane. The center of symmetry of each loop is not at $(h = 0, m = 0)$ but is shifted along the positive vertical axis; however, such a shift steadily goes to zero with increasing the number of iterations. The effect is observed at all angles (excluding $\phi = \pi/2$); two examples are shown in the top right panel of Figure 7.

In order to explain the nature of the anomaly and to provide a quantitative picture of the effect it is convenient to use the simplified rate equations when this is possible.

4.1. Simplified Rate Equations for Minor Loops

First, it is shown that when $h_v < 1$ and for an arbitrary value of ϕ the condition determining when rate equations can be applied in the simplified form (Equation (4)) does not only involve the temperature as previously discussed (Equation (5)) but also h_v and ϕ. Simplified equations can be

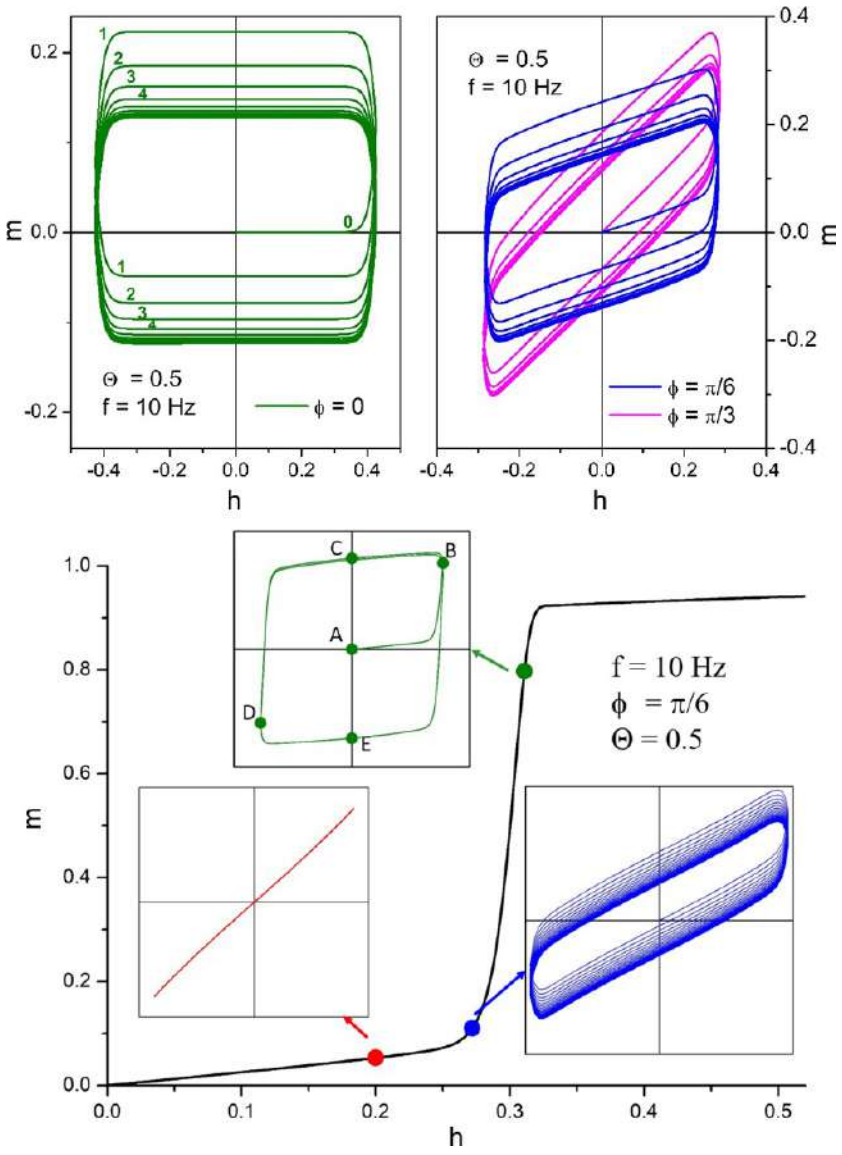

Figure 7: Top panels: minor loops of monodisperse nanoparticles for three ϕ angles. Bottom panel: first magnetization curve of an assembly of collinear monodisperse nanoparticles ($\phi = \pi/6$) well below blocking temperature at fixed magnetizing frequency (black line). Insets: shapes of minor hysteresis loops whose vertex fields are highlighted on the black line. Labels $A - E$ in the top inset show the states referred to in the text.

used when either τ_1^{-1} becomes negligible with respect to τ_2^{-1} or viceversa, the first condition applying to the case $h > 0$. It is possible to make this condition more quantitative by requiring, e.g., that $\tau_2^{-1} \geq 1 \times 10^3\, \tau_1^{-1}$ at the positive vertex field (where the largest possible difference between τ_1 and τ_2 is expected). With reference to the general definitions of τ_1^{-1} and τ_2^{-1} given in Section II.1 this requirement can be put in the form:

$$\epsilon_2(\phi, h_v) - \epsilon_1(\phi, h_v) \geq \frac{\Theta}{L} ln(1 \times 10^3) \approx 6.91 \frac{\Theta}{L} \tag{13}$$

the energies in the potential wells ϵ_i being:

$$\epsilon_i(\phi, h_v) = sin^2\theta_i(\phi) - 2h_v cos(\theta_i(\phi) - \phi)$$

For a given temperature Θ satisfying to Equation (5) the above condition is not fulfilled by all pairs of values of h_v and ϕ. Direct calculation shows that for a given vertex field h_v the angle ϕ cannot exceed an upper limit, as shown in Figure 8 where the shaded area contains the pairs of h_v, ϕ values satisfying to Equation (13) at two temperatures. In major loops ($h_v = 1$), the simplified rate equations can be applied at all angles.

When $\phi = 0$, $ln(\tau_1/\tau_0) = \frac{L}{\Theta}(1 + h_v)$ and $ln(\tau_2/\tau_0) = \frac{L}{\Theta}(1 - h_v)$ so that the condition reduces to:

$$h_v \geq 6.91 \frac{\Theta}{L}.$$

As an example, when $\Theta = 0.5$, h_v must be larger than about 0.14.

4.2. Loop anomaly

We consider a DWS assembly submitted to cyclic magnetization with positive vertex field h_v at frequency f and temperature Θ , all parameters being such that the simplified rate equations apply. Initially $h = 0$ and $m = 0$ (demagnetized state, point A in the upper inset, bottom panel of Figure 7; in this case the applied field is $h(t) = h_v sin(2\pi f t)$ and the states $B \rightarrow E$ are reached in sequence. The vertex magnetization on the first magnetization curve (point B) is $m_v^{[1]} = m(h_v)$; points C and E correspond to the upper and lowermagnetic remanence $m_{RUP}^{[1]}$, $m_{RLO}^{[1]}$ on the first loop. When the field reaches again the positive vertex a new loop begins.

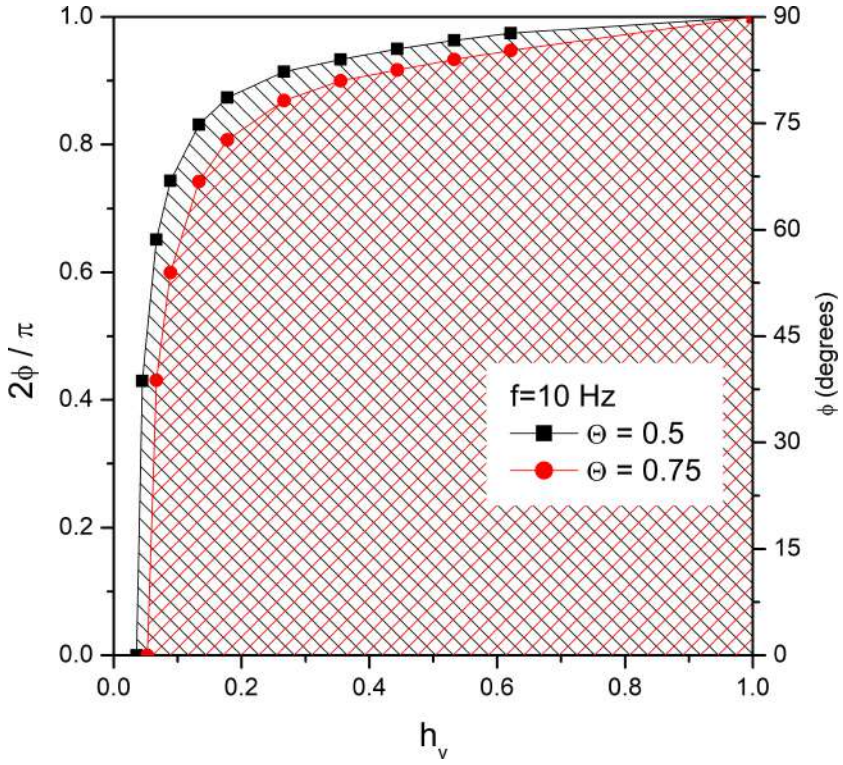

Figure 8: The shaded region contains all pairs of values of angle ϕ and vertex field h_v such that the simplified rate equations can be applied at the magnetizing frequency f and at two temperatures.

The general solutions of the simplified rate equations (Equation (8)) allow one to obtain the values of the upper and lower remanence $m_{RUP}^{[k]}$ and $m_{RLO}^{[k]}$ as functions of the number of iterations k. Detailed calculations are given in the Supplementary Material [73], Section 6. The result is:

$$m_{RUP}^{[k]} = \left\{1 - 2z\left[\frac{1-z^{2k-2}}{1+z} + \frac{1}{2}z^{2k-2}\right]\right\}cos\phi$$
$$m_{RLO}^{[k]} = \left\{1 - 2\left[\frac{1-z^{2k}}{1+z} + \frac{1}{2}z^{2k}\right]\right\}cos\phi \tag{14}$$

where $k = 1, 2, 3, ...$ is the number of loop interations and:

$$z = \frac{4}{\beta_\phi^2}(\alpha_\phi - m_v^{[1]})^2 \tag{15}$$

with $\alpha_\phi = cos(\theta_1(h_v) - \phi)$ and $\beta_\phi = [cos(\theta_1(h_v) - \phi) - cos(\theta_2(h_v) - \phi)]$. When $\phi = 0$, the simpler relation $z = (1 - m_v^{[1]})^2$ holds.
The typical behavior with k of $m_{RUP}^{[k]}$, $m_{RLO}^{[k]}$ and of their arithmetic mean $(m_{AV}^{[k]} = m_{RUP}^{[k]} + m_{RLO}^{[k]})/2$ is shown in the top panel of Figure 9 for two different values of h_v. The three quantities relax towards asymptotic values with a rate strongly increasing with increasing h_v. Large open symbols show the exact results obtained from the full rate equations, whereas the small symbols (perfectly superimposed to the previous ones) correspond to the prediction of Equation (14) deriving from the simplified rate equations. It should be remarked that in closed hysteresis loops the arithmetic mean of the remanences is zero, corresponding to loops centered in the origin. In fact, the two remanences become equal in absolute value and opposite in sign in the limit $k \to \infty$:

$$lim_{k\to\infty}\left[m_{RUP}^{[k]}\right] = \left(1 - \frac{2z}{1+z}\right)cos\phi = \frac{1-z}{1+z}cos\phi$$
$$lim_{k\to\infty}\left[m_{RLO}^{[k]}\right] = \left(1 - \frac{2}{1+z}\right)cos\phi = -\frac{1-z}{1+z}cos\phi \tag{16}$$

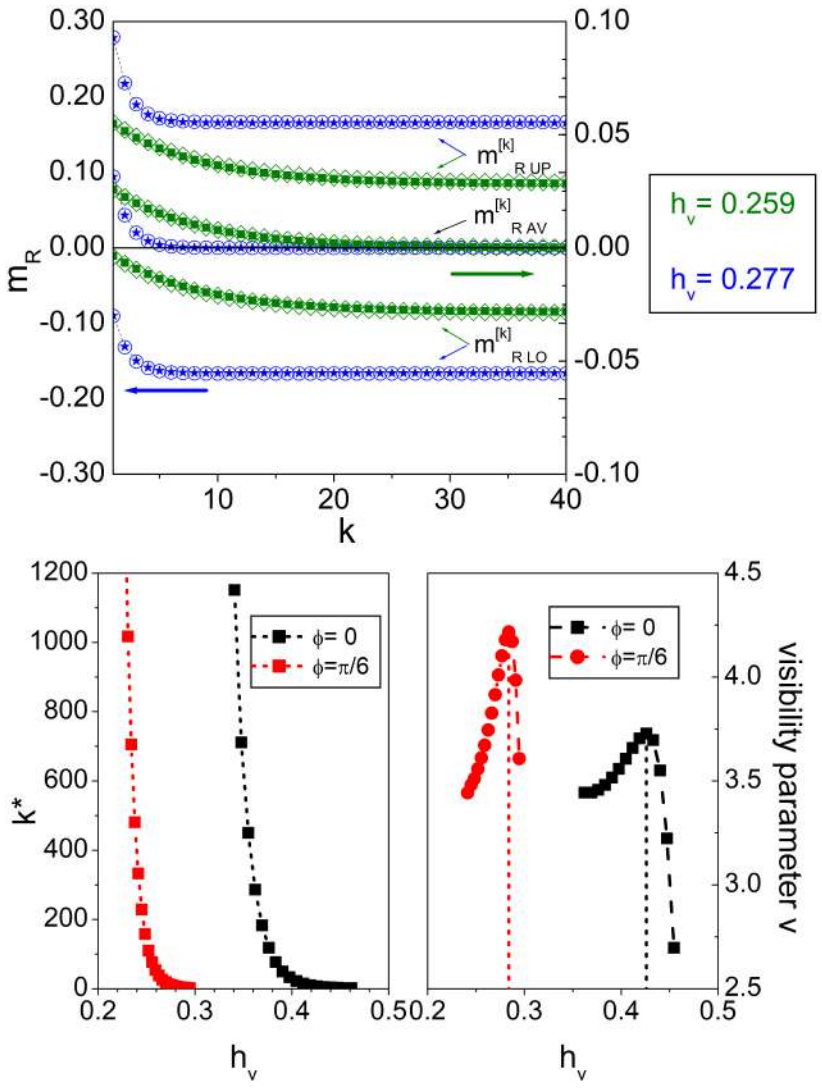

Figure 9: Top panel: upper/lower remanences $m^{[k]}_{RUP/LO}$ and arithmetic mean $m^{[k]}_{RAV}$ of minor loops with two different vertex fields h_v as functions of the number of iterations k for an assembly of collinear ($\phi = \pi/6$) monodisperse nanoparticles. Large open symbols: values resulting from the full rate equations; full symbols: values obtained from Equation (14). Bottom: number of iterations needed to reach the asymptotic remanences k^* (left panel) and visibility factor v (right panel; see Supplementary Material [73], Section 7) as functions of vertex field for two values of ϕ.

The following conclusions can be drawn:

a) in general, minor loops of a DWS assembly initially do not close on themselves: the arithmetic mean of the two remanences starts from a positive value and becomes zero only after an ideally infinite number of iterations; in other words, the system is self-adjusting and the spiral path initially followed by the magnetization in the (h, m) plane gradually transforms into a closed loop;

b) however, loops where $m_v^{[1]} \equiv \alpha_\phi$ are closed loops since the very beginning because $z = 0$ and there is no relaxation of the remanence. This condition amounts to say that the loop is a major loop for any angle ϕ ($\neq \pi/2$): in fact, Equation (1) shows that when h_v is such that $m_v^{[1]} = \alpha_\phi$ only one potential well survives and $n_{1\phi} = 1$; such a condition defines the major loop. As a consequence, major loops are stable for any ϕ; when $\phi = 0$ the condition for having a closed loop since the beginning becomes simpler: $m_v^{[1]} = 1$, i.e., $h_v \geq 1$;

c) the smaller the pair of (h_v, m_v) values is, the slower the system's relaxation. This is clearly shown in the bottom right panel of Figure 9 for two values of ϕ; there, k^* is the number of iterations needed to reach the asymptotic remanence values.

In order to establish a quantitative criterion to determine k^*, we introduce the relative variation $R^{[k]} = \left[\left(m_{RUP}^{[k]} + m_{RLO}^{[k]}\right)/\left(m_{RUP}^{[k]} - m_{RLO}^{[k]}\right)\right]$, which is a positive, monotonically decreasing function of k with asymptotic value $R^{[\infty]} = 0$ as easily proven by Equations (14) and (16). In this work, k^* is defined as the value of k at which $R^{[k]}$ becomes less than 1×10^{-3}.

Finally, it has been verified that the anomaly exists independently of the starting point of the loops. It should be noted that the limit $h_v \to 0$ cannot be properly investigated for two orders of reasons: *i*) the simplified rate equations no longer hold in this limit (see Section 4.1); *ii*) the loop becomes extremely narrow and cannot be resolved by numerically solving the rate equations.

A *visibility factor* for the loop anomaly can be defined, as shown in the Supplementary Material [73], Section 7.

5. Hysteresis Loops of a DWS Assembly with Random Easy Axis Directions

The behavior of a DWS assembly with randomly distributed easy axes is studied by averaging the solutions of the full rate equations (3) over all ϕ angles. In three dimensions, the average of a ϕ-dependent quantity $g(\phi)$ is the sum: $\sum_1^N g(\phi_i)sin(\phi_i)/\sum_1^N sin(\phi_i)$ over N angles in the interval $-\pi/2 \leq \phi_i \leq \pi/2$. In this work, N has been fixed to 181; the relative difference between the average done with $N = 181$ and with $N = 1801$ is negligible [39] ($< 2 \times 10^{-3}$).

5.1. Quasi-static conditions

5.1.1. Stored Energy

An expression for the energy of a system with randomly distributed easy axes is obtained starting from the general expression of the energy $\epsilon(\phi)$ stored in a collinear DWS assembly with arbitrary ϕ, i.e.:

$$\epsilon(\phi) = -2hm + \frac{sin^2\theta_1 - sin^2\theta_2}{cos(\theta_1 - \phi) - cos(\theta_2 - \phi)}m - \frac{sin^2\theta_1\, cos(\theta_2 - \phi) - sin^2\theta_2\, cos(\theta_1 - \phi)}{cos(\theta_1 - \phi) - cos(\theta_2 - \phi)} \tag{17}$$

as calculated in the Supplementary Material [73], Section 8. It is easily checked that Equation (17) reduces to $\epsilon = -2hm$ and $\epsilon = -h^2$ for $\phi = 0$ and $\phi = \pi/2$, respectively (see Section 3.4). The average over all ϕ values is reported in Figure 5 for $\Theta = 0.5$ and 1.15 (red lines). The same comments of Section 3.4 apply: in particular, during every half-cycle the magnetic energy is first stored in the DWS assembly and then quickly released to the environment at $h \approx |h_c|$. Averaging over all angles has the effect of somewhat reducing the amount of stored energy per cycle with respect to the collinear, $\phi = 0$ case; in fact, the best storage efficiency is associated to those particles

whose easy axis is aligned to the magnetic field so that a textured material with a dominant easy-axis direction would more efficient as a heat generator.

5.1.2. Curves of First Magnetization

The first magnetization curves of a system with randomly distributed easy axes are shown in Figure 10 in quasi-static conditions and for temperatures in the range $0 \leq \Theta \leq 1.15$. The result for $\Theta \to 0$ is coincident with the Stoner-Wohlfarth first magnetization curve, i.e., the average between upper and lower branch of the SW loop [1]. The sudden change in slope of $m(h)$ corresponds to the field where the change of occupancy numbers n_1 and n_2 is largest; the effect occurs at increasingly lower fields with increasing temperature; finally, when $\Theta > 1$ $m(h)$ becomes coincident with the equilibrium curve.

5.1.3. Effects of Temperature and Sweep Rate

The sweep rate r of the magnetic field has a detectable effect on the temperature dependence of the coercive field of a system whose kinetics is described by rate equations [59]. Figure 11 shows the $h_c(\Theta)$ curves for a monodisperse system obtained solving the full rate equations both in quasi-static conditions (reduced sweep rate r) and at a high frequency f. The curves become significantly less steep with increasing r or f. In quasi-static conditions, the considered r values have been chosen to result in actual sweep rates of $1 - 100$ Oe/s in measurements done on typical magnetite nanoparticles ($K_{eff} \approx 5 \times 10^5$ erg/cm^3, $M_s \approx 350$ emu/cm^3, $D \approx 7 \times 10^{-7}$ cm); this is basically the interval of instrumental sweep rates in quasi-static measurements done using a standard magnetometer.

In this range of r values, the $h_c(\Theta)$ curves obtained by solving the complete rate equations (open symbols in Figure 11) are well fitted by the following law:

$$|h_c| = 0.479\left\{1-\left(\frac{\Theta}{L}\right)^{\gamma}\left[-\frac{2}{\pi a}-\frac{ln(2x)}{2}+\sqrt{\left(\frac{2}{\pi a}+\frac{ln(2x)}{2}\right)^2-\frac{ln(2x)}{a}}\ \right]^{\gamma}\right\} \tag{18}$$

where $\gamma \simeq 0.77$ (full lines in Figure 11). This law is a straightforward generalization of Equation (9) valid for the $\phi = 0$ case, the argument x being

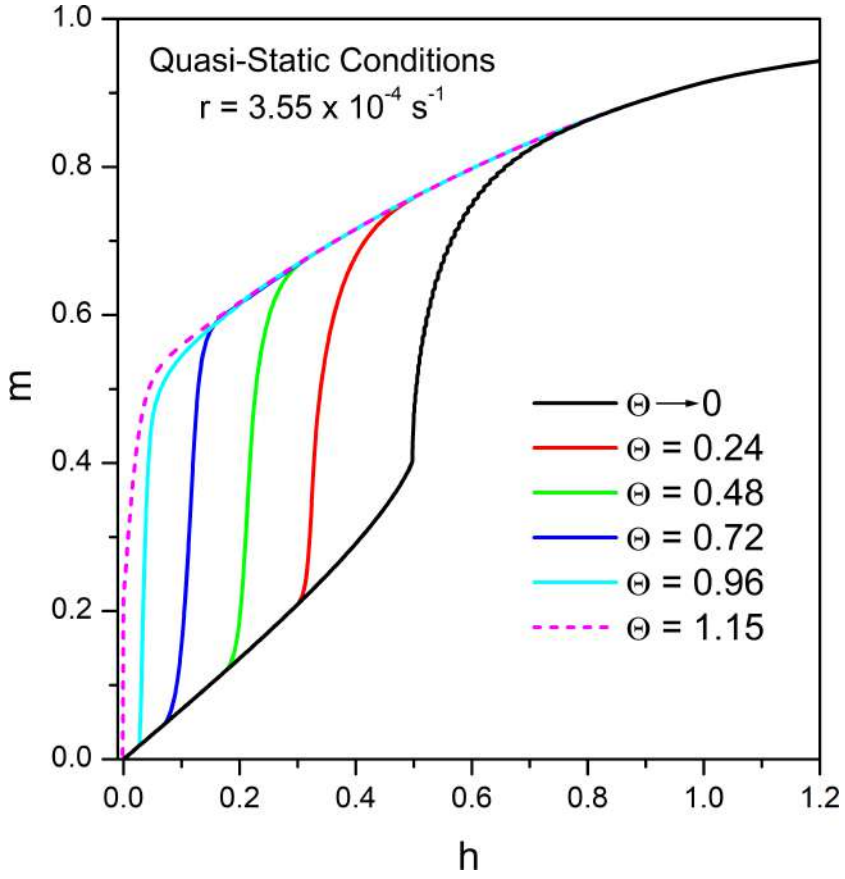

Figure 10: First magnetization curves of an assembly of monodisperse nanoparticles with random easy axes directions in quasi-static conditions at different temperatures. The dotted line for $\Theta = 1.15$ is the equilibrium curve.

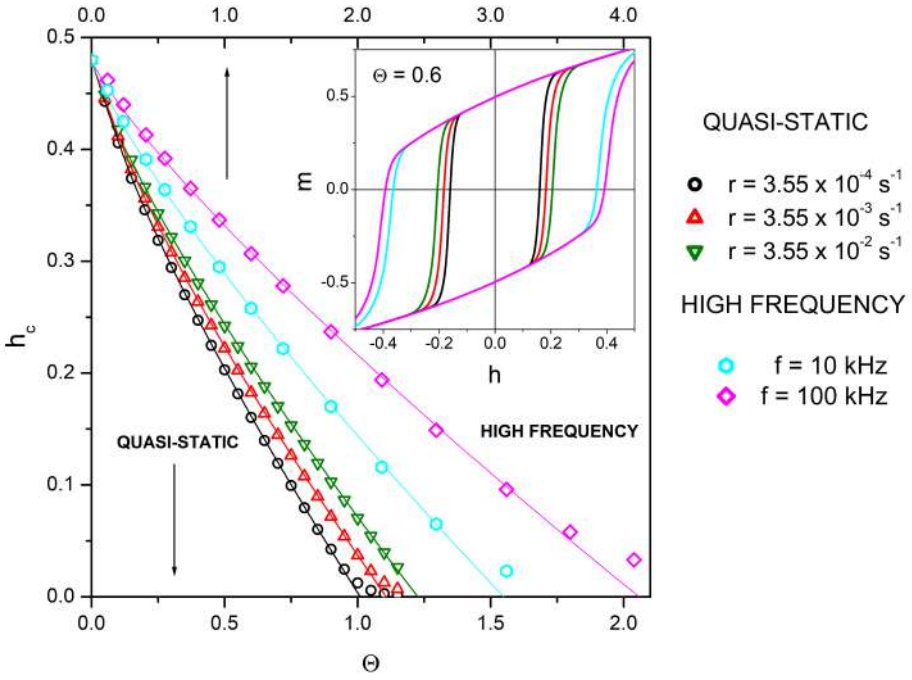

Figure 11: Temperature dependene of coercive field h_c for an assembly of monodisperse nanoparticles with random easy axes, for typical sweep rates of quasi-static measurements (bottom horizontal axis) and typical high frequencies (top horizontal axis). Symbols: results of full rate equations; lines: approximate analytic law (Equation (18)). Inset: shape of the corresponding hysteresis loops at fixed temperature.

defined as $x = \left[\frac{2}{\sqrt{\pi}}\left(\frac{L}{\Theta}\right)^{1/2}\tau_0 r ln2\right]$ as before. The approximate expression of the erf^{-1} function entering Equation (18) begins to lose validity near to $h_c = 0$ exactly as in the $\phi = 0$ case.

Interestingly, the same exponent $\gamma \simeq 0.77$ appears in the power law $h_c/h_c(0) = 1 - \Theta^{\gamma}$ proposed by Pfeiffer [65] for nanoparticles with randomly distributed easy axes, and often used in the analysis of experimental results [78, 79, 80, 81]. This exponent results from the analysis of thermal fluctuations when one considers the different effect of temperature on irreversible and reversible magnetization processes taking place in the nanoparticle assembly [65, 82]. A similar power law with $\gamma = 0.75$ was derived starting from the behavior of barrier energy with angle ϕ in the SW approximation [83]. However, these laws are not based upon a rate equation model and therefore do not take into account the effect of the rapidity at which the magnetic field changes. Our results clearly indicate that no simple power law of the type $h_c/h_c(0) = 1 - \Theta^{\gamma}$ is able to fit the true temperature behavior of the coercive field of an assembly of DWS with random easy axes. In fact, the shape of $h_c(\Theta)$ is markedly influenced by the sweep rate. Approximate expressions for $h_c(\Theta)$ derived from a rate equation approach and explicitly containing the sweep rate have been proposed[59, 66]; however, they are less effective than Equation (18) in reproducing the exact temperature dependence of coercivity in this range of r values.

The major hysteresis loops of the DWS assembly calculated well below blocking temperature ($\Theta = 0.6$) are reported in the inset of Figure 11 for the same sweep rates (line colors correspond to symbols in the main frame). The results clearly indicate that the most important effect of sweep rate is actually on h_c, while the kinetics of redistribution between the two energy wells is only marginally affected by a quasi-static sweep rate.

5.1.4. Effects of Size Distribution

The effect of a distribution of nanoparticle sizes on the hysteretic properties of a DWS assembly with random easy axis directions is shown in Figure 12. The size distribution is assumed to be lognormal with median diameter D_0 and shape parameter σ:

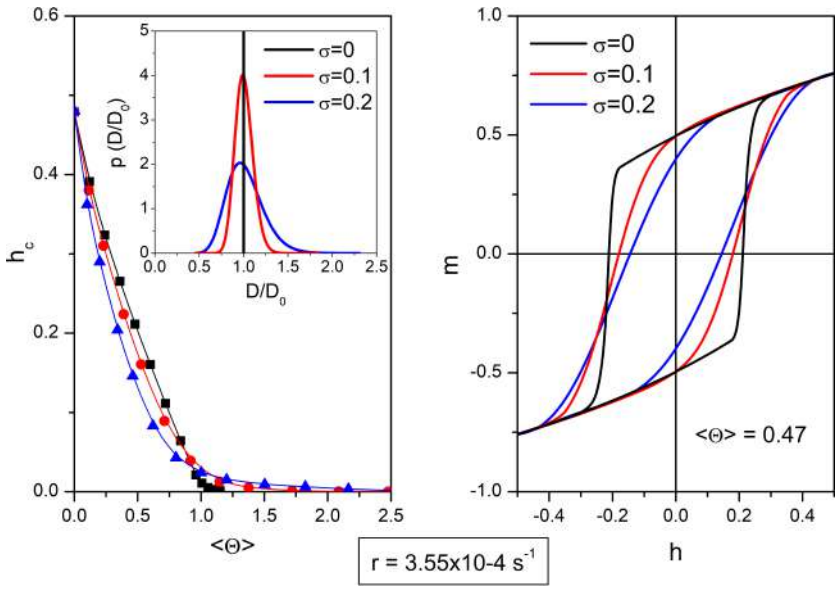

Figure 12: Left panel: effect of nanoparticle size distribution on the temperature behavior of the coercive field for an assembly of nanoparticles with random axes in quasi-static conditions. The corresponding $p(D)$ curves are shown in the inset. Right panel: effect of the distribution on the shape of major hysteresis loops at fixed temperature.

$$p(D/D_0) = \frac{1}{\sqrt{2\pi\sigma^2}} \frac{1}{(D/D_0)} e^{-\frac{ln^2(D/D_0)}{2\sigma^2}},$$

$\sigma = 0$ corresponding to a monodisperse system. The average blocking temperature $< T_B >$ is defined as the temperature where the particles of size $< D >$ become blocked. The behavior of h_c as a function of $< \Theta >= T/ < T_B >$ is shown in the left panel of Figure 12 for three values of σ (the corresponding $p(D)$ curves being displayed in the inset). The smooth monotonic behavior of $h_c(T)$ is generally preserved; however, the tail of the curve above $< \Theta >= 1$ becomes more pronounced with increasing σ because of the increasing contribution from larger nanoparticles still in the blocked state. On the contrary, at low $< \Theta >$ values the coercive field is lower for higher σ because of the increased influence of small NPs which become unblocked well below $< \Theta >= 1$. Increasing σ makes the hysteresis loops less steep and more slender in shape (an example is given in the right panel of Figure 12). The loop area decreases from $A_L = 0.440$ to $A_L = 0.345$ when the size distribution broadens ($\sigma = 0 \rightarrow \sigma = 0.2$). This is expained considering that the field region where the occupancy numbers n_1 and n_2 are modified by the rate equations becomes larger in a polydisperse system.

5.2. High frequency

Finally, the effect of frequency on the hysteretic properties of a monodisperse system with randomly distributed easy axes is shown in Fig. 13. Here, we limit ourselves to discuss major loops. The left panel shows the loops calculated at different frequencies for $\Theta = 0.5$. The curve calculated in quasi-static conditions is reported for comparison (dotted line). Increasing the frequency causes a shift of h_c towards higher values; the region of fields where the most important changes in occupancy numbers n_1, n_2 occur becomes slightly wider. Both effects contribute to the increase of the loop area with frequency reported in the right panel of Fig. 13. In the investigated region, the increase of loop area A_L is almost linear with the logarithm of f, corresponding to a power law of the type $A_L \propto f^{\zeta}$ with $\zeta \approx 0.03$.

The behavior of the coercive field as a function of temperature is well fitted by Equation (18) with the same exponent ($\gamma = 0.77$) even at high frequencies, as shown in Figure 11 for $f = 10$ and 100 kHz, corresponding to

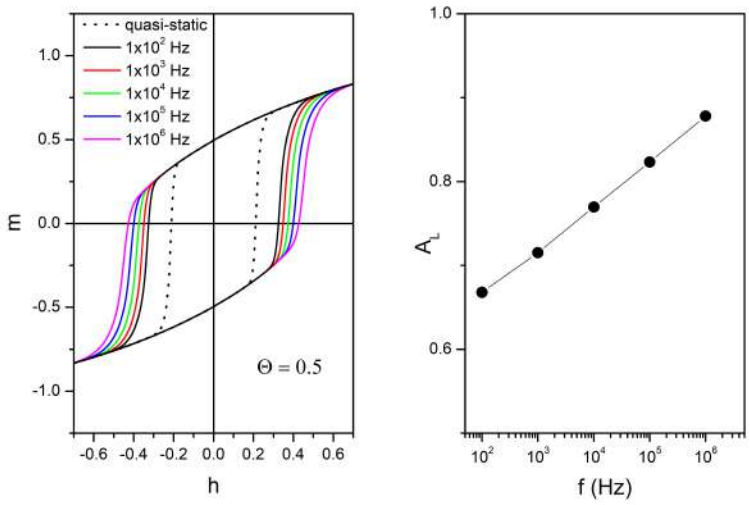

Figure 13: Left panel: effect of frequency on the shape of major loops for an assembly of nanoparticles with random easy axes at fixed temperature. Right panel: loop area A_L as a function of magnetizing frequency.

the typical operation range in magnetic hyperthermia applications. Therefore, Equation (18) is appropriate to describe the coercive field behavior of hysteresis loops measured in all types of experimental conditions.

It is remarkable that the expression of h_c for a random assembly of NPs (Equation (18)) is almost identical to the one for collinear DWS and $\phi = 0$ (Equation (9)), with the mere substitution of the exponent $\gamma = 1/2$ with $\gamma = 0.77$ exactly as in the formulas for h_c derived from Stoner-Wohlfarth theory[78].

6. Conclusions

A method based on rate equations has been applied to study magnetic hysteresis in an assembly of uniaxial nanoparticles described as double well systems. Although rate equations result from an approximation to magnetization dynamics in nanosystems, they allow an accurate picture of hysteresis

to be gained without much computational effort.

Rate equations can be further simplified by making special additional assumptions which hold for a large range of values of temperature, magnetic field and angle between field and easy axis. As a consequence, simple analytical expressions of significant quantities such as coercive field, magnetic energy, time lag of magnetization have been easily obtained in the case of collinear DWS. The analytical expressions given in this work can be applied over a very large range of magnetizing frequencies, including the ones typically used in practical applications of materials for magnetic hyperthermia.

A new expression for the temperature behavior of the coercive field, working at all frequencies of interest, has been derived in the case $\phi = 0$. This expression can be applied, in a slightly modified form, to the interesting case of an assembly of DWS with randomly oriented easy axes.

The phase shift between $m(t)$ and $h(t)$ at a given magnetizing frequency has been directly linked to the value of the coercive field at the same frequency, allowing the latter to be easily obtained in measurements done using a lock-in amplifier.

A distinctive anomaly has been observed in minor hysteresis loops and quantitatively expained. Simplified rate equations allow one to deduce analytical laws and to predict the condition of maximum visibility of the effect. From a fundamentalist′s viewpoint, the effect is interesting because it shows how much does the kinetics of population redistribution impact on a system′s ability to reach the steady state under the effect of a steady driving force.

Such an anomaly turns out to be certainly non-negligible in loops whose vertex fields are much lower than the coercive field. This is the usual condition when operating at high frequencies in a typical experiment of magnetic hyperthermia: in that case vertex fields are rather low for technical reasons related to the response of magnetizing coils, whereas the coercive field is much larger than in quasi-static measurements, as shown in this work; therefore the condition $h_v << h_c$ is usually met in hyperthermia measurements, so that this anomalous effect is hardly an academic issue.

A random distribution of easy axes preserves all features observed in the collinear system while somewhat smoothing the effects. At high frequency, the area of a major loop increases with frequency according to a power law.

A distribution of nanoparticle sizes $p(D)$ brings about changes in the behavior of coercive field with temperature, shape of the loop and loop area. In particular, the wider the size distribution is, the smaller the loop area. However, the size distribution of nanoparticles has probably less effect on the hysteretic properties than on the FC/ZFC curves whose features are extremely dependent on mean value and width of $p(D)$.

In conclusion, simplified rate equations describe the hysteretic behavior of an assembly of non-interacting magnetic nanoparticles in a most satisfactory way, the simplifications involved in the model being useful to reduce the complexity of the problem without significantly distorting the underlying physics. The results of the present study can also be applied to the important case of weakly interacting nanoparticles where the effect of interparticle interaction can be described by an effective field theory, and can serve as a starting point in the description of magnetic hysteresis in strongly interacting NP systems where magnetization reversal is a collective process rather than the result of independent events.

[1] E. C. Stoner and E. P. Wohlfarth, Philos. T. R. SOC. S-A **240**, 599 (1947).

[2] E. F. Kneller and F. E. Luborsky, J. Appl. Phys. **34**, 656, (1963).

[3] B. D. Cullity and C. D. Graham, *Introduction to Magnetic Materials* (IEEE press, Wiley, 2009), Ed. 2.

[4] A. E. Berkowitz, F. T. Parker, F. E. Spada and D. Margulies in *Magnetic Properties of Fine Particles* edited by J. L. Dormann and D. Fiorani (North-Holland Delta Series, 1992), Chapter 8, pp. 309-322.

[5] Q. A. Pankhurst, BT Technol. J. **14**, 33, (2006).

[6] I. Koh and L. Josephson, Sensors **9**, 8130, (2007).

[7] A. Bhargava, N. Jain and J. Panwar in *Current topics in biotechnology and microbiology* edited by H. K. Dhingra, P. N. Jha and P. Bajpai (Lambert Academic Publishing, 2011), Chapter 6, pp117-155.

[8] M. Colombo, S. Carregal-Romero, M. F. Casula, L. Gutierrez, M. P. Morales, I. B. Bohm, J. T. Heverhagen, D. Prosperi and W. J. Parak, Chem. Soc. Rev. **41**, 4306, (2012).

[9] L. Xie, R. Jiang, F. Zhu, H. Liu and G. Ouyang, Anal. Bioanal. Chem. **406**, 377, (2014).

[10] A. Sobczak-Kupiec, J. Venkatesan, A. A. AlAnezi, D. Walczyk, A. Farooqi, D. Malina, S. H. Hosseinie and B. Tyliszczak, Nanomed-Nanotechnol **12**, 2459, (2016).

[11] C. Banerjee, S. Choudhury, J. Sinha and A. Barman, Phys. Rev. Appl. **8**, 014036, (2017).

[12] P. Chureemart, R. F. L. Evans, R.W. Chantrell, P.-W. Huang, K. Wang, G. Ju, and J. Chureemart, Phys. Rev. Appl. **8**, 024016, (2017).

[13] M. Angelakeris, Biochim. Biophys. Acta, **1861**, 1642, (2017).

[14] T. Marzi, R. Meckenstock, S. Masur and M. Farle, Phys. Rev. Appl., **10**, 054002, (2018).

[15] S. Bagheri, N. M. Julkapli, J. Magn. Magn. Mater. **416**, 117, (2016).

[16] H. Shokrollahi, J. Magn. Magn. Mater. **426**, 74, (2017).

[17] M. Branca, M. Marciello, D. Ciuculescu-Pradines, M.Respaud, M. del Puerto Morales, R.Serra, M-J. Casanove, C. Amiens, J. Magn. Magn. Mater. **377**, 348, (2015).

[18] M. Knobel, W. C. Nunes, L. M. Socolovsky, E. De Biasi, J. M. Vargas and J. C. Denardin, J. Nanosci. Nanotechnol. **8**, 2836 (2008).

[19] S. Bedanta, A. Barman, W. Kleemann, O. Petracic and T. Seki, J. Nanomater. **2103**, 952540, (2013).

[20] D. Lisjak and A. Mertelj, Prog. Mater. Sci. **95**, 286 (2018).

[21] C. Binns, *Nanomagnetism: Fundamentals and Applications* (Elsevier, 2014), Vol. 6.

[22] S. P. Gubin, *Magnetic Nanoparticles* (Wiley-VCH, 2009).

[23] K. D. Sattler, *Handbook of Nanophysics: Nanoparticles and Quantum Dots* (CRC Press, 2011), Vol. 3.

[24] O. Moscoso-Londoño, P. Tancredi, D. Muraca, P. Mendoza Zélis, D. Corald, M.B. Fernández van Raap, U. Wolff, V. Neu, C. Damm, C.L.P. de Oliveira, K.R. Pirota, M. Knobel, L.M. Socolovsky, J. Magn. Magn. Mater. **428**, 105, (2017).

[25] B. Mehdaoui, A. Meffre, J. Carrey, S. Lachaize, L.-M. Lacroix, M. Gougeon, B. Chaudret, and M. Respaud, Adv. Func. Mater. **21**, 4573, (2011).

[26] N. A. Usov and B. Y. Liubimov, J. Appl. Phys. **112**, 023901, (2012).

[27] K. Simeonidis, M. P. Morales, M. Marciello, M. Angelakeris, P. de la Presa, A. Lazaro-Carrillo, A. Tabero, A. Villanueva, O. Chubykalo-Fesenko and D. Serantes, Sci. Rep. **6**, 38382, (2016).

[28] Z. Hedayatnasab, F. Abnisa, W. M. A. W. Daud, Materials and Design, **123**, 174, (2017).

[29] Z. Shaterabadi, G. Nabiyouni, M. Soleymani, Prog. Biophys. Mol. Bio. **133**, 9, (2018).

[30] M-K. Kim, J. Sim, J-H. Lee, M. Kim and S-K. Kim, Phys. Rev. Appl. **9**, 054037, (2018).

[31] W. Aadinath, T. Ghosh, C. Anandharamakrishnan, J. Magn. Magn. Mater. **401**, 1159, (2016).

[32] M.L. Tebaldi, C.M.R. Oda, L.O.F. Monteiro, A.L.B. de Barros, C. J. Santos, D.C. Ferreira Soares, J. Magn. Magn. Mater. **461**, 116, (2018).

[33] P. Allia, G. Barrera and P. Tiberto, Phys. Rev. Applied, in press (2019)

[34] N-N. Song, H-T. Yang, H-L. Liu, X. Ren, H-F. Ding, X-Q. Zhang and Z-H. Cheng, Sci. Rep. **3**, 3461, (2013).

[35] D. Soto-Aquino and C. Rinaldi, J. Magn. Magn. Mater. **393**, 46, (2015).

[36] O. A. Inozemtseva, S. V. German, N. A. Navolokin, A. B. Bucharskaya, G. N. Maslyakova and D. A. Gorin in *Nanotechnology and Biosensors* edited by D. P. Nikolelis and G-P. Nikoleli (Elsevier,2018), Chapter 6.

[37] I. Morales, R. Costo, N. Mille, G. B. da Silva, J. Carrey, A. Hernando and P. de la Presa, Nanomaterials, **8**, 970, (2018).

[38] L. Néel, Ann. Geophys. (C.N.R.S.), **5**, 99 (1949).

[39] P. Allia, G. Barrera and P. Tiberto, Phys, Rev, B **98**, 134423 (2018).

[40] A. P. Guimaraes, *Principles of Magnetism* (Springer, 2009).

[41] K. H. J. Buschow, *Handbook of Magnetic Materials* (Elsevier,2015), Vol. 23.

[42] K. Trohidou, *Magnetic Nanoparticle Assemblies* (Pan Stanford Publishing 2014).

[43] N. A. Usov and Yu. B. Grebenshchikov, J. Appl. Phys. **105**, 043904 (2009).

[44] W. F. Brown Jr. Phys. Rev. **130**, 1677, (1963).

[45] Y. P. Kalmykov, J. Appl. Phys. **96**, 1138, (2004).

[46] D. Peddis, P. E. Jonsson, S. Laureti and G. Varvaro in *Nanomagnetism: Fundamentals and Applications* edited by C. Binns (Elsevier, 2014) Vol. 6, Chapter 4, pp. 129-188.

[47] S. Chakraverty, M. Bandyopadhyay, S. Chatterjee, S. Dattagupta, A. Frydman, S. Sengupta and P. A. Sreeram, Phys. Rev. B **71**, 054401 (2005).

[48] M. Bandyopadhyay and S. Dattagupta, Phys. Rev. B **74**, 214410 (2006).

[49] M. Sasaki, P. E. Jonsson, H. Takayama and H. Mamiya, Phys. Rev. B **71**, 104405 (2005).

[50] G. M. Tsoi, L. E. Wenger, U. Senaratne, R. J. Tackett, E. C. Buc, R. Naik, P. P. Vaishnava and V. Naik, Phys. Rev. B **72**, 014445 (2005).

[51] N. A. Usov, J. Appl. Phys. **109**, 023913 (2011)

[52] N. A. Usov, J. Appl. Phys. **107**, 123909, (2010).

[53] T. J. Fal, M. L. Plumer, J. P. Whitehead, J. I. Mercer, J. van Ek and K. Srinivasan, Appl. Phys. Lett. **102**, 202404, (2013).

[54] W. T. Coffey, D. S. F. Crothers, Yu. P. Kalmykov, E. S. Massawe and J. T. Waldron, Phys. Rev. E **49**, 1869, (1994).

[55] J. L. Garcia-Palacios and F. J. Lazaro, Phys. Rev. B **58**, 14937, (1998).

[56] W. Scholz, T. Schrefl and J. Fidler, J. Magn. Magn. Mater. **49**, 296, (2001).

[57] D. A. Garanin, E. C. Kennedy, D. S. F. Crothers and W. T. Coffey, Phys. Rev. E **60**, 6499, (1999).

[58] W.T. Coffey, D.A. Garanin, H. Kachkachi, D.J. McCarthy, J. Magn. Magn. Mater. **221**, 110, (2000).

[59] N. A. Usov and Yu. B. Grebenshchikov, J. Appl. Phys. **106**, 023917, (2009).

[60] W. C. Nunes, W. S. D. Folly, J. P. Sinnecker, and M. A. Novak, Phys. Rev. B **70**, 014419, (2004).

[61] V. Franco and A. Conde, J. Magn. Magn. Mater. **278**, 28, (2004)

[62] E. De Biasi, R.D. Zysler, C.A. Ramos and M. Knobel, J. Magn. Magn. Mater. **320**, e312, (2008)

[63] E. De Biasi, C.A. Ramos and R.D. Zysler, J. Magn. Magn. Mater. **353**, 105, (2014)

[64] I. Petrila and A. Stancu, J. Phys.: Condens. Matter **23**, 076002, (2011)

[65] H. Pfeiffer, phys. stat. sol. (a) **118**, 295 (1990).

[66] J. Carrey, B. Mehdaoui, and M. Respaud, J. Appl. Phys. **109**, 083921, (2011).

[67] A. A. Timopheev, S. M. Ryabchenko, V. M. Kalita, A. F. Lozenko, P. A. Trotsenko, V. A. Stephanovich, A. M. Grishin and M. Munakata, J. Appl. Phys. **105**, 083905, (2009).

[68] I. Petrila, I. Bodale, C. Rotarescu and A. Stancu, Phys. Lett. **A375**, 3478, (2011)

[69] J.M.D.Coey, *Magnetism and Magnetic Materials* (Cambridge University Press, 2009).

[70] A. G. Roca, G. Vallejo-Fernández and K. O'Grady, IEEE T. Magn. **47**, 2878, (2011).

[71] L-M. Lacroix, R. Bel Malaki, J. Carrey, S. Lachaize, M. Respaud, G. F. Goya and B. Chaudret, J. Appl. Phys. **105**, 023911, (2009).

[72] J. J. Lu, H. L. Huang and I. Klik, J. Appl. Phys. **76**, 1726, (1994).

[73] See the Supplementary Material for calculation details, a study of the phase shift in high-frequency measurements and a definition of the loop-anomaly visibility factor.

[74] S. Winitzki, A handy approximation for the error function and its inverse, https://drive.google.com/file/d/0B2Mt7luZYBrwZlctV3A3eF82VGM/view (2008).

[75] H.T. Karlsson and I. Bjerle, Comp. Chem. Engineering **4**, 67 (1980).

[76] C. Hastings, Jr., *Approximations for Digital Computers* (Princeton University Press, Princeton, 1955) p. 185.

[77] T. Sato, K. Nagaoka, S. Kobayashi, J. Manjanna, and Takeshi Murakami, AIP Advances **7**, 056319 (2017).

[78] X. Batlle, M. García del Muro, J. Tejada, H. Pfeiffer, P. Görnert, and E. Sinn J. Appl. Phys **74**, 3333 (1993).

[79] E. F. Ferrari, W. C. Nunes, and M. A. Novak, J. Appl. Phys. **86**, 3010 (1999).

[80] P.K. Choudhury, S. Banerjee, S. Ramaprabhu, K. P. Ramesh, and R. Menon, J. Nanosci. Nanotech. **13**, 8162 (2013).

[81] A. López-Ortega, E. Lottini, C. de Julián Fernández, and C. Sangregorio, Chem. Mater. **27**, 4048 (2015).

[82] B.T.Shirk and W.R.Buessem, IEEE Trans. Magn. **7**, 659 (1971).

[83] J. García-Otero, A.J. García-Bastida, and J. Rivas, J. Mag. Magn. Mater. **189**, 377 (1998).

SUPPLEMENTARY MATERIAL TO:

HYSTERESIS EFFECTS IN MAGNETIC NANOPARTICLES: A SIMPLIFIED RATE-EQUATION APPROACH

Paolo Allia [1,2], Gabriele Barrera [1], Paola Tiberto [1]

[1] *INRIM, Advanced Materials Metrology and Life Sciences, Strada delle Cacce 91, 10135 Torino (TO), Italy*

[2] *DISAT, Politecnico di Torino, Corso Duca degli Abruzzi 24, I-10129 Torino, Italy*

---

1 - Ratio L/Θ in Frequency Measurements

In measurements done at frequency f the blocking temperature T_{Bf} is defined by the relation $L_f k_B T_{Bf} = K_{eff} V$ where $L_f = ln(1/(f\tau_0))$; as a consequence the blocking temperature of a DWS assembly increases with respect to the static ($f \to 0$) blocking temperature T_B, so that at any T the reduced temperature $\Theta_f = T/T_{Bf}$ is smaller than $\Theta = T/T_B$; however the ratio L_f/Θ_f turns out to be independent of f because

$$\frac{L_f}{\Theta_f} = \frac{L_f T_{Bf}}{T} = \frac{K_{eff} V}{k_B T} = \frac{L T_B}{T} = \frac{L}{\Theta}$$

where $L = ln(\tau_{meas}/\tau_0) = ln(100/\tau_0) \simeq 25$ is the conventional relation valid for quasi-static measurements.

2 - Explicit Calculation of h_c for $\phi = 0$

On the upper half of a major loop, h continuously decreases from $h_v = 1$ to $h_v = -1$. Well below T_B the potential energy well (1) is completely filled

$(h_v = 1 \rightarrow n_{10} = 1, m = 1)$. The coercive field on the loop's upper branch h_c is defined as the negative field such that $m = 0$, i.e., $n_{10} = 1/2$. Therefore, the first of Equations 8 of the main text becomes:

$$\frac{1}{2} = exp\Big(\frac{1}{\tau_0 r_{RMS}} \int_1^{h_c} e^{-\frac{L}{\Theta}(1+h)^2} dh\Big)$$

where $h_c < 0$; the equation transforms to:

$$\int_{h_c}^{1} e^{-\frac{L}{\Theta}(1+h)^2} dh = \tau_0 r_{RMS} ln2$$

Making the substitution of variable $\frac{L}{\Theta}(1+h)^2 = u^2$ one has:

$$\int_{h_c}^{1} e^{-\frac{L}{\Theta}(1+h)^2} dh = \Big(\frac{\Theta}{L}\Big)^{1/2} \int_{(\Theta/L)^{1/2}(1+h_c)}^{2(\Theta/L)^{1/2}} e^{-u^2} du =$$

$$= \frac{\sqrt{\pi}}{2}\Big(\frac{\Theta}{L}\Big)^{1/2} \left\{ erf\left[2\Big(\frac{L}{\Theta}\Big)^{1/2}\right] - erf\left[\Big(\frac{L}{\Theta}\Big)^{1/2}(1+h_c)\right]\right\} = \tau_0 r_{RMS} ln2$$

It is possible to put $erf\Big[2\Big(\frac{L}{\Theta}\Big)^{1/2}\Big] = 1$ because the argument is considerably larger than unity for all Θ values of interest here; therefore:

$$erf\left[\Big(\frac{L}{\Theta}\Big)^{1/2}(1+h_c)\right] = 1 - \frac{2}{\sqrt{\pi}}\Big(\frac{L}{\Theta}\Big)^{1/2} \tau_0 r_{RMS} ln2$$

This relation allows one to express h_c as:

$$h_c = -1 + \Big(\frac{\Theta}{L}\Big)^{1/2} erf^{-1}\left[1 - \frac{2}{\sqrt{\pi}}\Big(\frac{L}{\Theta}\Big)^{1/2} \tau_0 r_{RMS} ln2\right]$$

Recalling the definition of r_{RMS}, h_c becomes:

$$h_c = -1 + \Big(\frac{\Theta}{L}\Big)^{1/2} erf^{-1}\left[1 - \Big(\frac{L}{\Theta}\Big)^{1/2} \tau_0 f ln2\right]$$

The coercive field on the upper loop branch turns out to be a negative quantity, as expected. By analogy, the coercive field on the lower loop branch is:

$$h_c = 1 - \left(\frac{\Theta}{L}\right)^{1/2} erf^{-1}\left[1 - \left(\frac{L}{\Theta}\right)^{1/2} \tau_0 f ln2\right]$$

When $x = \left(\frac{L}{\Theta}\right)^{1/2} \tau_0 f ln2$ is much smaller than one, the approximate expression of the erf^{-1} function [2] reported in Equation (9) of main text can be applied. In fact, the condition $x \ll 1$ is valid even for very small Θ values; for example when $f = 1$ MHz, Θ must be larger than about 10^{-5} (an easily satisfied condition) in order to use Equation (9).

3 - Phase Shift in High-Frequency Measurements

In typical high-frequency measurements, the system′s response is measured as a function of time by applying a sinusoidal waveform $h(t)$ [1]. Here, the field is supposed to be initially at the positive vertex of a major loop ($h_v = 1$); therefore, $h(t) = cos(\omega t)$ where $\omega = 2\pi f$. According to Equation (10) of main text the magnetization is $m(h) = 2n_{10}(h) - 1$; initially $n_{10} = 1$ and $m = +1$. The $m(t)$ waveform is obtained using the simplified rate equations 4 of the main text; $h(t)$ and $m(t)$ are plotted as functions of time in the left panel of Fig. 1 for $\Theta = 0.5$. A time lag between the two waveforms appears; its amount can be evaluated by looking for the time t^* for which $h = h_c$ on the upper branch:

$$h_c(f) = cos(\omega t^*) \qquad \rightarrow \qquad t^* = \frac{1}{2\pi f} arccos[h_c(f)]$$

Note that $t^* > T/4$ ($T = 1/f$ being the waveform's period) because h_c is a negative quantity. In a very narrow time interval around $t = t^*$ well (1) is emptied ($n_{10} \rightarrow 0$) and $m \rightarrow -1$. Therefore, when m is plotted as a function of t the first zero is at $t = t^*$ whereas the first zero of $h(t)$ is at $t = T/4$ (see Figure 1). The time lag of $m(t)$ with respect to $h(t)$ is:

$$\Delta_t = \frac{1}{2\pi f} arccos\big[h_c(f)\big] - \frac{1}{4f}$$

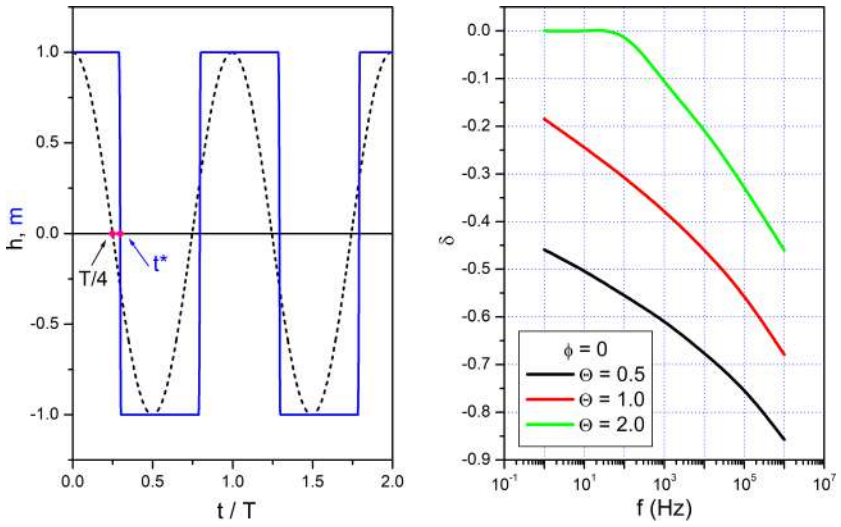

Figure 1: Left panel: time evolution of the magnetization of collinear monodisperse nanoparticles ($\phi = 0$) (full line) under a harmonic magnetic field $h(t)$ (dotted line); the resulting time lag is indicated by red dots. T is the waveform's period. Right panel: phase shift δ between $h(t)$ and $m(t)$ as a function of magnetizing frequency.

and the associated phase shift $\delta = \omega\Delta_t$ is

$$\delta = arccos\big[h_c(f)\big] - \frac{\pi}{2} \tag{SM.1}$$

The behavior of δ as a function of frequency is reported in the right panel of Figure 1 for three different values of Θ. The shift increases in absolute value with increasing f, as expected. Above blocking temperature, the phase shift appears when the hysteresis loop opens. It should be remarked that Equation (SM.1) of the Supplementary Material file allows one to evaluate the coercive field h_c by measuring the phase shift δ. This can be very useful in high-frequency measurements, when it can be experimentally much simpler to quickly get the phase shift (e.g., using a lock-in analyzer) rather than to measure a full hysteresis loop.

4 - Explicit Calculation of the First Magnetization Curve for $\phi = 0$

The first magnetization curve of a DWS assembly is defined as the path followed by the system's magnetization by effect of an increasing positive field h starting from the demagnetized state ($h = m = 0; \quad n_{10} = n_{20} = 1/2$). In close analogy with the procedure developed in Section 2 of this Supplementary Material, the argument of the exponential in Equation (11) of main text transforms to:

$$-\frac{1}{\tau_0 r_{RMS}} \int_0^h e^{\frac{L}{\Theta}(1-h)^2} dh = -\frac{1}{\tau_0 r_{RMS}} \Big(\frac{\Theta}{L}\Big)^{1/2} \int_{(1-h)(\frac{L}{\Theta})^{1/2}}^{(\frac{L}{\Theta})^{1/2}} e^{-u^2} du.$$

Following the steps reported in Section 2, this expression becomes the $-\beta(h)$ function given in Equation (12) of main text.

5 - Approximate formula for the erf Function

The following approximation for the erf function [3] has been used in Section 3.5 of the main text:

$$erf(x) \approx 1 - \Big[a_1\Big(\frac{1}{1+a_4 x}\Big) + a_2\Big(\frac{1}{1+a_4 x}\Big)^2 + a_3\Big(\frac{1}{1+a_4 x}\Big)^3\Big] e^{-x^2}$$

with

$$a_1 = 0.3480242; \quad a_2 = -0.0958798; \quad a_3 = 0.7478556; \quad a_4 = 0.4704700.$$

The absolute error between exact and approximate values of the erf function is less than 2×10^{-5} [3].

6 - Iterative Expression of Magnetic Remanence at all ϕ Angles

With reference to the loop points indicated in the upper inset, bottom panel of Figure 7 of the main text, the evolution of n_{10} and/or n_{20} will here be followed during the transformation $A \to B \to C \to D \to E \to B$ involving: a) the first magnetization curve from the demagnetized state A to the upper vertex B and b) the first complete loop.
The general solutions shown in Equation (8) of main text apply. As an example, in the $A \to B \to C$ transformation $n_{2\phi}$ varies in the following way:

$$\begin{aligned}
&in\ A: \qquad n_{2\phi}(0) = \frac{1}{2} \\
&in\ B: \qquad n_{2\phi}(h_v) = \frac{1}{2} exp\Big(- \frac{1}{r_{RMS}} \int_0^{h_v} \frac{1}{\tau_2} dh \Big) \\
&in\ C: \qquad n_{2\phi}(0) = \Big[\frac{1}{2} exp\Big(- \frac{1}{r_{RMS}} \int_0^{h_v} \frac{1}{\tau_2} dh \Big) \Big]\ exp\Big(+ \frac{1}{r_{RMS}} \int_{h_v}^{0} \frac{1}{\tau_2} dh \Big).
\end{aligned}$$

The change in sign in the argument of the rightmost exponential of the last line arises from the change in sign of the rate r_{RMS}. The general property $\tau_1(-h) = \tau_2(h)$ implies some identities among integrals entering the solutions (8) when applied to different segments of the transformation. In particular, defining:

$$
\begin{aligned}
I_{A\to B} &= exp\Big(-\frac{1}{r_{RMS}} \int_0^{h_v} \frac{1}{\tau_2} dh \Big) \\
I_{B\to C} &= exp\Big(+\frac{1}{r_{RMS}} \int_{h_v}^{0} \frac{1}{\tau_2} dh \Big) \\
I_{C\to D} &= exp\Big(+\frac{1}{r_{RMS}} \int_0^{-h_v} \frac{1}{\tau_1} dh \Big) \\
I_{D\to E} &= exp\Big(-\frac{1}{r_{RMS}} \int_{-h_v}^{0} \frac{1}{\tau_1} dh \Big)
\end{aligned}
\tag{SM.2}
$$

where the change of sign of r_{RMS} between transformations done with increasing/decreasing h has been taken in due account, one gets:

$$
I_{A\to B} = I_{B\to C} = I_{C\to D} = I_{D\to E} \equiv z^{1/2}
$$

having introduced the quantity $z = I^2_{A\to B}$. Note that $0 < z < 1$ for any h_v. It is now easy to get the evolution of the occupancy numbers $n^{[k]}_{1\phi}$ and/or $n^{[k]}_{2\phi}$ with the number of loop iterations k by making repeated use of Equations (8) of hte main text. In point A, $n_{2\phi} = 1/2$; therefore:

$$
\begin{aligned}
&in \quad B: \qquad n^{[1]}_{2\phi} = \frac{1}{2} z^{1/2} \\
&in \quad C: \qquad n^{[1]}_{2\phi} = \frac{1}{2} z \qquad \longrightarrow \qquad n^{[1]}_{1\phi} = 1 - \frac{1}{2} z \\
&in \quad D: \qquad n^{[1]}_{1\phi} = z^{1/2} - \frac{1}{2} z^{3/2} \\
&in \quad E: \qquad n^{[1]}_{1\phi} = z - \frac{1}{2} z^2 \qquad \longrightarrow \qquad n^{[1]}_{2\phi} = 1 - z + \frac{1}{2} z^2 \\
&in \quad B: \qquad n^{[1]}_{2\phi} = z^{1/2} - z^{3/2} + \frac{1}{2} z^{5/2}
\end{aligned}
\tag{SM.3}
$$

where label [1] indicates that these are the values on the first loop. Each of the transformation's segments has the effect of multiplying the expression

for the relevant occupancy number $n_{i\phi}$ $(i = 1, 2)$ by $z^{1/2}$. We are interested in determining the upper and lower magnetic remanence, i.e., the magnetization at points C and E. On the first loop $(k = 1)$, the above expressions give the following values for the two remanences:

$$m^{[1]}_{RUP} = \big(1 - 2n^{[1]}_{2\phi}\big)cos\phi = (1 - z)cos\phi$$
$$m^{[1]}_{RLO} = \big(2n^{[1]}_{1\phi} - 1\big)cos\phi = (-1 + 2z - z^2)cos\phi = -(1 - z)^2 cos\phi$$

By simple iteration, the remanences of the k-th loop are found to be:

$$m^{[k]}_{RUP} = \Big[1 - 2z\Big(1 - z + z^2 - ... - z^{2k-3} + \frac{1}{2}z^{2k-2}\Big)\Big]cos\phi =$$
$$= \Big[1 - 2z\Big(\frac{1 - z^{2k-2}}{1 + z} + \frac{1}{2}z^{2k-2}\Big)\Big]cos\phi$$

$$m^{[k]}_{RLO} = \Big[1 - 2\Big(1 - z + z^2 - ... - z^{2k-1} + \frac{1}{2}z^{2k}\Big)\Big]cos\phi =$$
$$= \Big[1 - 2\Big(\frac{1 - z^{2k}}{1 + z} + \frac{1}{2}z^{2k}\Big)\Big]cos\phi$$

where use has been made of the formula for the sum of a geometric progression of ratio $(-z)$. These expressions are valid for all ϕ angles $\neq \pi/2$ and are coincident with the ones appearing in Equation (14) of main text. In particular, if $z = 0$ one has $m^{[k]}_{RUP} = cos\phi$, $m^{[k]}_{RLO} = -cos\phi$ while for $z = 1$ one has $m^{[k]}_{RUP} = m^{[k]}_{RLO} = 0$. For $0 < z < 1$ both remanences are monotonically decreasing functions of the iteration number k.

Finally, there is no need of actually calculating the parameter z from the integrals of Equation (SM.2). In fact, z can be easily related to the magnetization $m^{[1]}_v = m^{[1]}(h_v)$ evaluated in the upper vertex (point B) on the first magnetization curve $(A \to B)$; from the first of Equations (SM.3) one has:

$$z = 4n_{2\phi}^2 \tag{SM.4}$$

whereas the magnetization in B on the first magnetization curve is:

$$m_v^{[1]} = cos(\theta_1 - \phi) - \big[(cos(\theta_1 - \phi) - cos(\theta_2 - \phi)\big] n_{2\phi}^{[1]} \equiv \alpha_\phi - \beta_\phi n_{2\phi}^{[1]}. \tag{SM.5}$$

Equation (15) of main text directly follows from Equations (SM.4) and (SM.5).

7 - Visibility Factor for the loop anomaly

The whole range of possible loop shapes is summarized by the three insets in the bottom panel in Figure 7 of main text: small minor loops (red curve) are so narrow that the anomaly (although large) is hardly visible; almost major loops (green curve) are basically closed and stable; the anomaly if most apparent at intermediate h_v values (blue curve). This suggest one to define a visibility factor v in the following way:

$$v = k^* \Big(m_{RUP}^{[\infty]} - m_{RLO}^{[\infty]} \Big) = 2k^* \, \frac{1-z}{1+z} cos\phi$$

where k^* is the number of iterations needed to reach stability and $\big(m_{RUP}^{[\infty]} - m_{RLO}^{[\infty]}\big)$ is a measure of the loop width. These two quantites have opposite behavior as functions of h_v, so that their product exhibits a sharp maximum univocally indicating the vertex field where loop **anomaly** is best observed. The visibility factor is shown in the bottom right panel of Figure 9 of main text for $\phi = 0$ and $\phi = \pi/6$.

8 - Magnetic Energy of a Collinear DWS Assembly at all ϕ Angles

The general expression of the magnetic energy $\epsilon(\phi) = n_{1\phi}\epsilon_1(\phi) + n_{2\phi}\epsilon_2(\phi)$ is obtained using Equation (1) of main text which implies that:

$$n_{1\phi} = \frac{m(\phi) - c_2}{c_1 - c_2}$$
$$n_{2\phi} = -\frac{m(\phi) - c_1}{c_1 - c_2}$$

where $c_i = cos(\theta_i - \phi)$. The energies of the two energy wells are $\epsilon_i = s_i^2 - 2hc_i$ where $s_i^2 = sin^2\theta_i$. After simple steps the total magnetic energy $\epsilon(\phi)$ turns out to be:

$$\epsilon(\phi) = -2hm(\phi) + \frac{s_i^2 - s_2^2}{c_1 - c_2} m(\phi) - \frac{s_1^2 c_2 - s_2^2 c_1}{c_1 - c_2}$$

which is coincident with Equation (17) of main text.

[1] N. A. Usov and B. Y. Liubimov, J. Appl. Phys. **112**, 023901, (2012).

[2] S. Winitzki, A handy approximation for the error function and its inverse, https://drive.google.com/file/d/0B2Mt7luZYBrwZlctV3A3eF82VGM/view (2008).

[3] H.T. Karlsson and I. Bjerle, Comp. Chem. Engineering **4**, 67 (1980).